1990-09

Analysis of loss for inductive strips in finline

Kurtoglu, Levent

Monterey California. Naval Postgraduate School

NAVAL POSTGRADUATE SCHOOL
Monterey, California

THESIS

ANALYSIS OF LOSS FOR INDUCTIVE
STRIPS IN FINLINE

by

Levent Kurtoglu
September, 1990

Thesis Advisor: Jeffrey B. Knorr

Approved for public release; distribution is unlimited.

REPORT DOCUMENTATION PAGE

Form Approved OMB No. 0704-0188

1a REPORT SECURITY CLASSIFICATION: UNCLASSIFIED	1b RESTRICTIVE MARKINGS
2a. SECURITY CLASSIFICATION AUTHORITY	3 DISTRIBUTION / AVAILABILITY OF REPORT: Distribution unlimited
2b. DECLASSIFICATION / DOWNGRADING SCHEDULE	
4. PERFORMING ORGANIZATION REPORT NUMBER(S)	5 MONITORING ORGANIZATION REPORT NUMBER(S)
6a. NAME OF PERFORMING ORGANIZATION: Naval Postgraduate School; 6b OFFICE SYMBOL (If applicable): EW	7a NAME OF MONITORING ORGANIZATION: Naval Postgraduate School
6c. ADDRESS (City, State, and ZIP Code): Monterey, CA 93943-5000	7b ADDRESS (City, State, and ZIP Code): Monterey, CA 93943-5000
8a. NAME OF FUNDING / SPONSORING ORGANIZATION; 8b. OFFICE SYMBOL (If applicable)	9 PROCUREMENT INSTRUMENT IDENTIFICATION NUMBER
8c. ADDRESS (City, State, and ZIP Code)	10 SOURCE OF FUNDING NUMBERS: PROGRAM ELEMENT NO; PROJECT NO; TASK NO; WORK UNIT ACCESSION NO.

11. TITLE (Include Security Classification)
ANALYSIS OF LOSS FOR INDUCTIVE STRIPS IN FINLINE

12. PERSONAL AUTHOR(S)
KURTOGLU, Levent

13a TYPE OF REPORT	13b TIME COVERED	14 DATE OF REPORT (Year, Month, Day)	15 PAGE COUNT
Master's thesis	FROM _____ TO _____	1990 September	69

16 SUPPLEMENTARY NOTATION The views expressed in this thesis are those of the author and do not reflect the official policy or position of the Department of Defense or the U.S. Government.

17 COSATI CODES			18 SUBJECT TERMS (Continue on reverse if necessary and identify by block number)
FIELD	GROUP	SUB-GROUP	Finline, Inductive Strip, Finline Discontinuity, Ohmic Losses.

19 ABSTRACT (Continue on reverse if necessary and identify by block number)

This thesis introduces the effect of the loss to the homogeneous finline strip model. The expressions for the Quality Factors associated with the ohmic losses for inductive strips in homogeneous finline are derived and included in the CAD compatible circuit model in terms of the finite Q inductances. It is shown that the lossy circuit models more accurately predict the experimental response of an X band finline filter.

20 DISTRIBUTION / AVAILABILITY OF ABSTRACT	21 ABSTRACT SECURITY CLASSIFICATION
☒ UNCLASSIFIED/UNLIMITED ☐ SAME AS RPT ☐ DTIC USERS	UNCLASSIFIED
22a NAME OF RESPONSIBLE INDIVIDUAL: KNORR, Jeffrey E.	22b TELEPHONE (Include Area Code): 408-646-2815; 22c OFFICE SYMBOL: EC/KO

DD Form 1473, JUN 86 — Previous editions are obsolete — S/N 0102-LF-014-6603

Approved for public release; distribution is unlimited.

Analysis of Loss
for Inductive Strips in Finline

by

Levent Kurtoglu
Lieutenant Junior Grade, Turkish Navy

Submitted in partial fulfillment
of the requirements for the degree of

MASTER OF SCIENCE IN SYSTEM ENGINEERING
(Electronic Warfare)

from the

NAVAL POSTGRADUATE SCHOOL
September 1990

Author: [redacted]
Levent Kurtoglu

Approved by: [redacted]
Prof. Jeffrey B. Knorr, Thesis Advisor

[redacted]
Prof. R. Janaswamy, Second Reader

[redacted]
Joseph Stenberg, Chairman
EW Academic Group

ABSTRACT

This thesis introduces the effect of the loss to the homogeneous finline strip model. The expressions for the Quality Factors associated with the ohmic losses for inductive strips in homogeneous finline are derived and included in the CAD compatible circuit model in terms of the finite Q inductances. It is shown that the lossy circuit models more accurately predict the experimental response of an X band finline filter.

TABLE OF CONTENTS

I. INTRODUCTION

A. BACKGROUND

Integrated finline was first introduced as a low-loss transmission line by Paul J. Meier in 1974 [Ref.1]. Finline is superior to microstrip in many respects for millimeter wavelengths. Advantages include low-loss, low-cost, suppression of higher mode propagation, wide useful bandwidth, simple interfacing with waveguide circuits and eased production tolerances.

Since finline has many advantages it has found a wide range of applications in millimeter wave engineering. A unilateral finline configuration is shown in Figure 1 below.

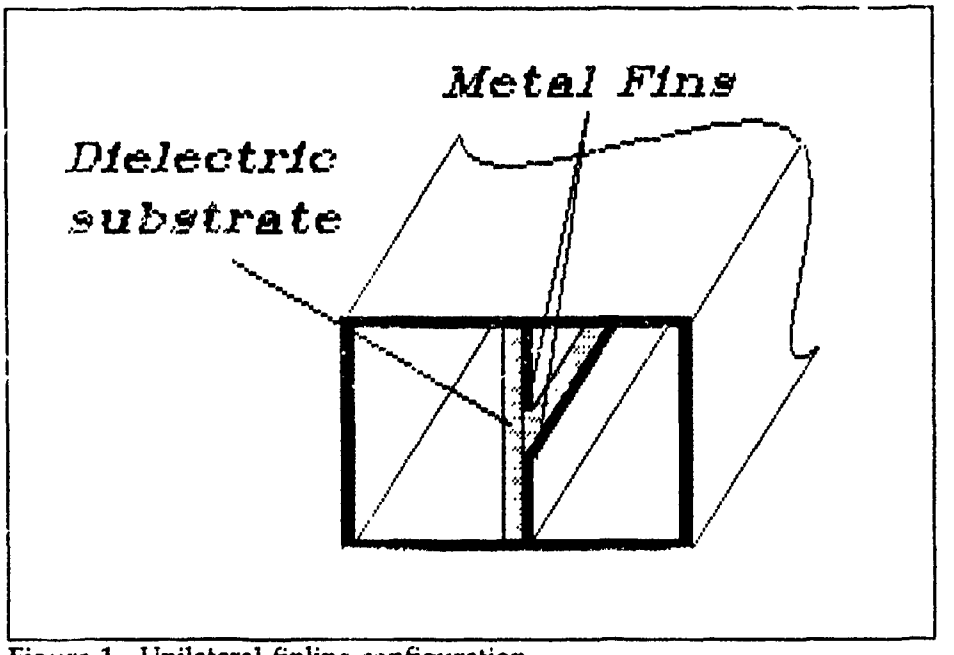

Figure 1. Unilateral finline configuration.

In its most general form, finline has metallic fins printed onto a thin dielectric slab that allows the processing of complex millimeter wave circuits on a single dielectric substrate. The substrate is then inserted in the electric field plane of a dominant mode rectangular waveguide. The finline structure where no dielectric substrate is used is called homogeneous finline.

Figure 2 shows an inductive strip in a finline structure. It is a primary element used in the design of finline filters.

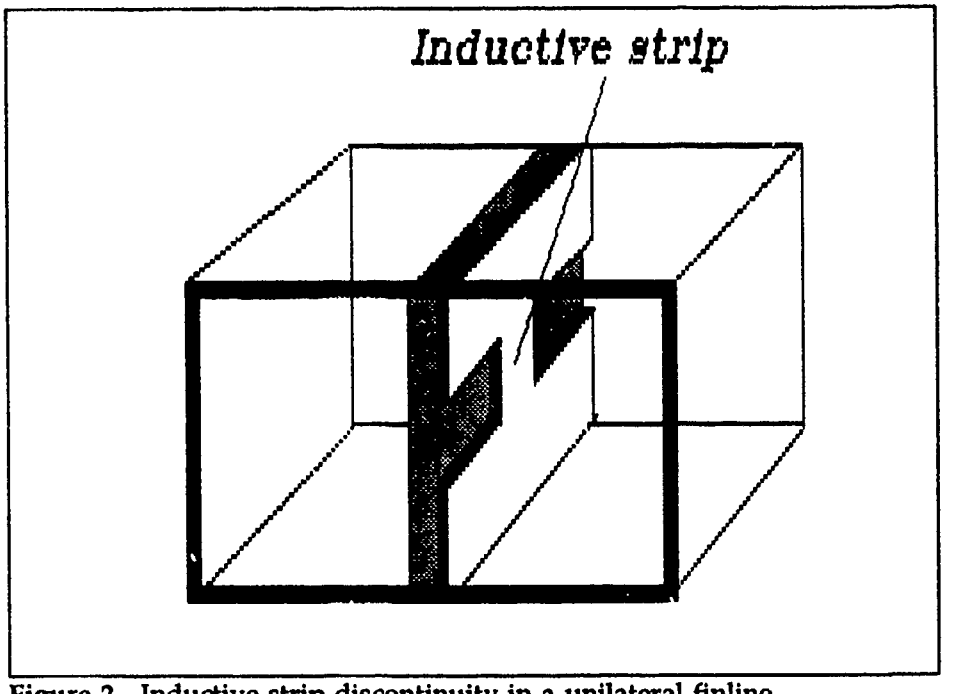

Figure 2. Inductive strip discontinuity in a unilateral finline.

For practical applications of this important finline discontinuity, simple and accurate equivalent circuit models were developed by Jeffrey B. Knorr. These are well suited for CAD [Ref.2].

Figure 3 presents one of the circuit models for the inductive strip in homogeneous finline [page 28 in Ref.2]. It simply

consists of two below-cutoff waveguide sections representing the space on each side of the strip extending up to the guide wall and two inductances that model the strip edge discontinuity.

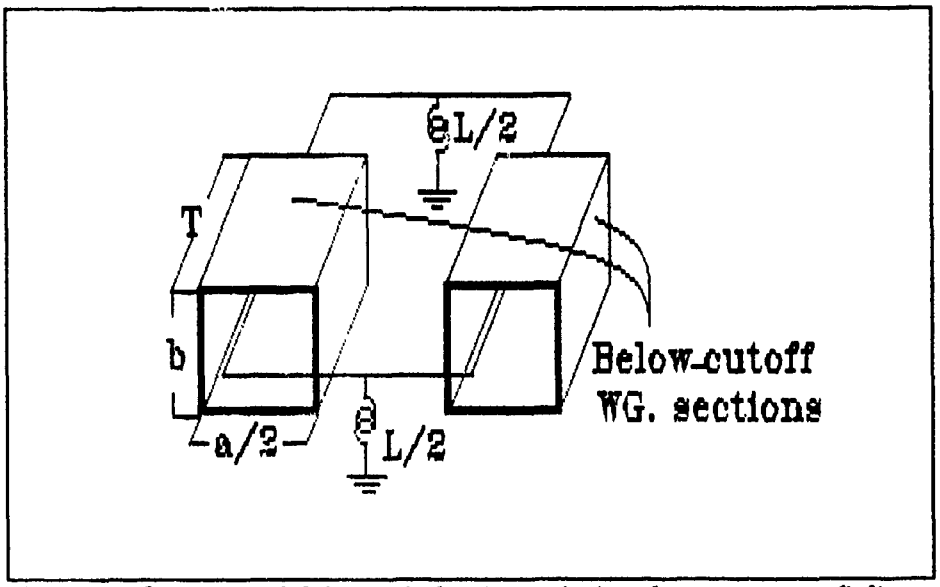

Figure 3. Circuit model for an inductive strip in a homogeneous finline.

B. RELATED WORK

Numerous studies of finline and the inductive strip discontinuity have been conducted by Jeffrey B. Knorr and his thesis students in the last decade at the Naval Postgraduate School.

The first study describes the spectral domain analysis of finline and was published by Knorr and Shayda in 1980 [Ref.3]. A thesis by Kim presents the equations and computer program listing for the generation of the numerical data [Ref.4]. Spectral domain analysis of scattering from an inductive strip in finline was described by Knorr and Deal in 1985 [Ref.5]. A computer program described in Deals thesis was used to generate

numerical scattering coefficients for the strip discontinuity [Ref.6].

The equivalent circuit models for a lossless inductive strip in homogeneous finline, on which this thesis is based, were described by Knorr in his 1988 and 1990 technical reports [Ref.7-2].

C. PURPOSE

The losses associated with the inductive strip in homogeneous finline are the TE_{10} mode ohmic losses due to the finite surface resistivity of the metal walls in the below-cutoff sections and the higher order mode ohmic losses associated with the currents generated by the strip edge discontinuity. The purpose of this thesis is to develop analytical expressions for the inductive strip losses in homogeneous finline; to include the effect of the loss in the equivalent circuit model and to establish the validity of the model by demonstrating better agreement between the experimental and predicted scattering response of a lossy X-band finline filter.

Chapter II of this thesis describes the derivation of the power loss expression in a semi-infinite waveguide below cutoff. Chapter III describes the derivation of the Quality Factor for the below cutoff waveguide section. Chapter IV describes the derivation of the leading edge loss and related Quality Factor expression. Chapter V describes the introduction of the loss to the equivalent circuit model of the inductive strip, and finally, Chapter VI presents conclusions and recommendations for future studies

II. LOSS IN A SEMI-INFINITE WAVEGUIDE BELOW CUTOFF

The loss concept for the inductive strip in homogeneous finline can be analyzed in two parts; wall losses, and the edge losses.

Associated wall losses occur in the regions that are modeled by the two below-cutoff waveguide sections in Figure 3. In this chapter, the power loss term in a semi infinite below-cutoff waveguide will be developed for further circuit modeling.

A. A DISCUSSION ON THE ABOVE AND BELOW CUTOFF WAVEGUIDE MODES

Figure 4 shows a rectangular waveguide which is a hollow metallic pipe, with a rectangular cross section of inner dimensions a and b. As a single conductor system, a rectangular waveguide cannot support TEM waves which need two or more conductors. It is capable of supporting TE and TM modes.

The cutoff frequency for a rectangular waveguide can be defined as the minimum operating frequency at which propagation of energy is possible without severe attenuation. In the above-cutoff region the propagation constant, $\gamma=\alpha+j\beta$, of a lossless guide is imaginary. Practically, attenuation of the fields occurs from the dissipative loss due to the finite resistivity of the imperfect metallic walls and finite conductivity of the imperfect dielectric insulator. These losses cause the propagation constant to become complex with real part $\alpha>0$. In the below-cutoff region where frequencies from zero frequency to the cutoff frequency are

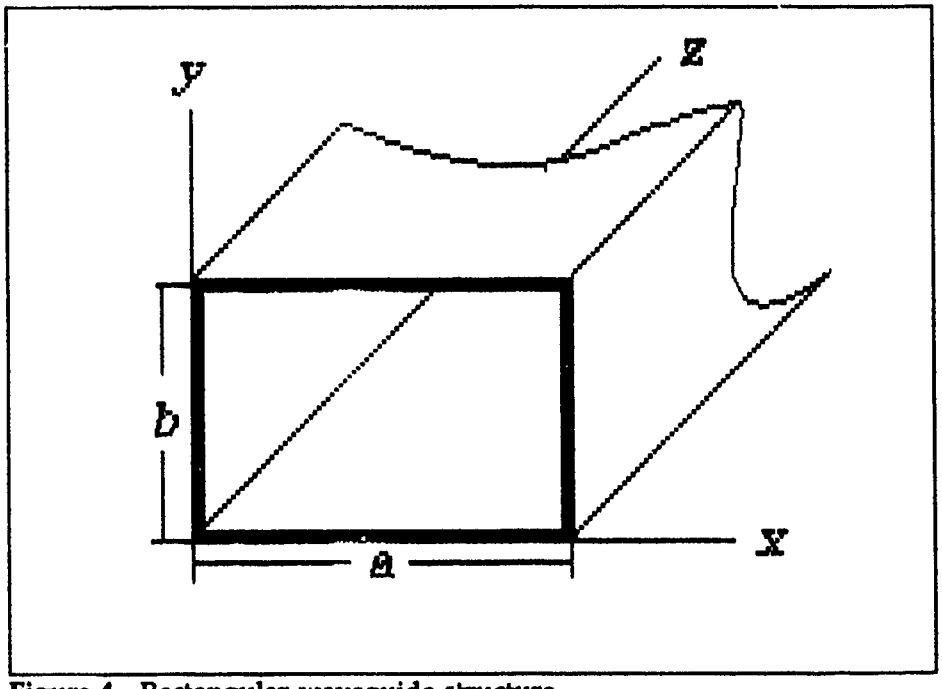

Figure 4. Rectangular waveguide structure.

included, the propagation constant, γ , of a lossless guide is real. Below-cutoff modes are called evanescent waveguide modes and can be represented by non-propagating, localized electromagnetic fields with amplitudes that decay rapidly due to the real propagation constant as a function of distance. Practically, at a moderate distance from the interface the only existing mode is the TE_{10} evanescent mode. All other evanescent modes are attenuated severely in shorter distances due to their larger propagation constants relative to TE_{10} evanescent mode. Since the below-cutoff guide walls are not perfect conductors the confined fields (evanescent modes) will suffer ohmic losses. Further discussion of evanescent modes is given in Chapter III, Part A.

B. REFLECTION COEFFICIENT AT A BOUNDARY BETWEEN THE ABOVE AND BELOW CUTOFF SECTIONS

Figure 5 shows a lossless semi-infinite rectangular waveguide consisting of two regions that are filled with dielectric and air. This dielectric discontinuity is used to excite evanescent TE_{10} mode in the air region. The further analysis shows that the Q factor derived for below-cutoff air region is independent of the dielectric constant of the dielectric region.

For TE_{10} mode propagation, the cutoff frequencies for the dielectric region (Region 1) and the air region (Region 2) are given by

$$f_{c1}=\frac{\frac{c}{\sqrt{\epsilon_r}}}{2a} \qquad (1)$$

$$f_{c2}=\frac{c}{2a} \qquad (2)$$

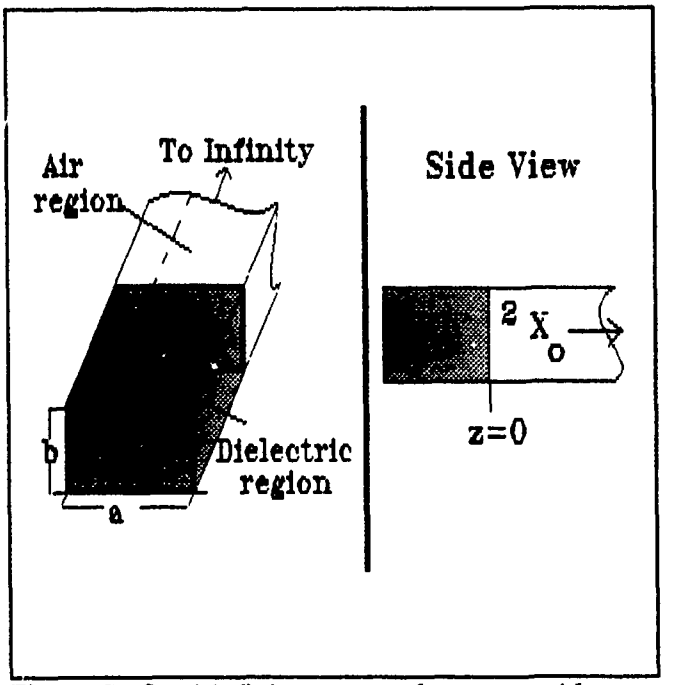

Figure 5. Semi-infinite rectangular waveguide.

where subscripts 1 and 2 denote the dielectric and air regions, respectively. In the operating frequency region between the two cutoff frequencies ($f_{c1}<f<f_{c2}$), the excited dominant mode is evanescent in the air-filled section, but is propagated in the dielectric-filled section. In other words the dielectric-filled section is above

cutoff whereas the air filled section is below cutoff for the TE_{10} waveguide mode.

The characteristic impedance for the dielectric region is real and is given by,

$$R_{o1}=\frac{\sqrt{\frac{\mu_o}{\epsilon_o\epsilon_r}}}{\sqrt{1-(\frac{f_{c1}}{f})^2}}. \tag{3}$$

The characteristic impedance of the air region is imaginary and is $Z_{02}=jX_{02}$ where,

$$X_{o2}=\frac{\sqrt{\frac{\mu_o}{\epsilon_o}}}{\sqrt{(\frac{f_{c2}}{f})^2-1}}. \tag{4}$$

By utilizing the characteristic impedance of each region, the reflection coefficient at the boundary can be derived as,

$$\Gamma=\frac{jX_{o2}-R_{o1}}{jX_{o2}+R_{o1}}=-\frac{R_{o1}-jX_{o2}}{R_{o1}+jX_{o2}}=1\ \angle(2\arctan(\frac{X_{o2}}{R_{o1}})) \tag{5}$$

where,

$$\frac{X_{o2}}{R_{o1}}=\sqrt{\frac{\epsilon_r-(\frac{f_{c2}}{f})^2}{(\frac{f_{c2}}{f})^2-1}} \tag{6}$$

In reality, due to the finite conductivity of the walls in the air filled section, the evanescent TE_{10} mode suffers dissipative loss. Under these circumstances the characteristic impedance looking into the below cutoff guide is not purely imaginary but has a real part that accounts for the ohmic losses, and is defined as $Z_{02}=R_{02}+jX_{02}$. Using this definition of the characteristic impedance, the reflection coefficient at the boundary between the above and below cutoff sections assumes a value which is slightly less than unity. The reflection coefficient with loss is given by,

$$\Gamma'=\frac{jX_{02}+R_{02}-R_{01}}{jX_{02}+R_{02}+R_{01}} \tag{7}$$

where,

$$|\Gamma'|^2 < |\Gamma|^2=1 \tag{8}$$

and the transmission coefficient at the interface z=0 is

$$|T|^2=(1-|\Gamma'|^2)>0\ . \tag{9}$$

The results obtained above show that at the boundary some of the energy is transferred to the air region and the TE_{10} evanescent mode is set up by the TE_{10} propagating mode in the dielectric-filled region.

C. FIELD EXPRESSIONS

1. Field expressions for the above-cutoff region

In the structure shown in Figure 5, the TE_{10} dominant mode is excited at operating frequency f where $f_{c1}<f<f_{c2}$. In region 1 the propagation constant is imaginary if the attenuation of fields due to the ohmic losses are ignored. It is expressed as,

$$\gamma_1 = j\beta_1 \tag{10}$$

where the phase constant is,

$$\beta_1 = \frac{2\pi}{\lambda_0}\sqrt{\epsilon_r}\sqrt{1-(\frac{f_{c1}}{f})^2}\ . \tag{11}$$

The electromagnetic wave pattern in the dielectric region is the superposition of the forward and the reflected waves that are propagating in the z and -z directions, respectively. Hence, the electric field for region 1 may be expressed as,

$$E_{y1} = E_{11}\sin\pi\frac{x}{a}e^{-j\beta_1 z} + \Gamma E_{11}\sin\pi\frac{x}{a}e^{+j\beta_1 z}\ . \tag{12}$$

The corresponding magnetic fields can be obtained by using the general relationship,

$$\overline{H} = \frac{j}{w\mu}\overline{\nabla}\times\overline{E}. \tag{13}$$

Taking the curl of the electric field vector yields,

$$\overline{H} = \frac{j}{w\mu}[(\frac{\partial E_z}{\partial y} - \frac{\partial E_y}{\partial z})\overline{a}_x + (\frac{\partial E_x}{\partial z}) - (\frac{\partial E_z}{\partial x})\overline{a}_y + (\frac{\partial E_y}{\partial x} - \frac{\partial E_x}{\partial y})\overline{a}_z]\ . \tag{14}$$

Since the TE_{10} mode has only a transverse electric field component in the y direction, the partial derivatives of the other electric field components can be dropped from Eq.14. This gives,

$$\overline{H} = \frac{j}{w\mu}[-(\frac{\partial E_y}{\partial z})\overline{a}_x + (\frac{\partial E_y}{\partial x})\overline{a}_z]\ . \tag{15}$$

Thus,

$$H_{x1} = -\frac{j}{w\mu}\frac{\partial E_{y1}}{\partial z} \tag{16}$$

$$H_{z1} = \frac{j}{w\mu}\frac{\partial E_{y1}}{\partial x} \tag{17}$$

and substitution of Eq.12 into Eq.16 and Eq.17 and taking the partial derivatives in the given directions yields the final expressions for the longitudinal and transverse magnetic field components as,

$$H_{x1} = -\frac{\beta}{w\mu}[E_{11}\sin\frac{\pi x}{a}e^{-j\beta_1 z} - \Gamma E_{11}\sin\frac{\pi x}{a}e^{+j\beta_1 z}] \tag{18}$$

$$H_{z1} = \frac{j}{w\mu}[k_x(E_{11}\cos\frac{\pi x}{a}e^{-j\beta_1 z} + \Gamma E_{11}\cos\frac{\pi x}{a}e^{+j\beta_1 z})] \ . \tag{19}$$

2. Field expressions for the below-cutoff region

As stated in previous sections, the transmitted portion of the TE_{10} waveguide mode from the above cutoff region establishes the TE_{10} evanescent mode in the below-cutoff region. In the lossless case, it is attenuated with a real propagation constant that can be expressed as,

$$\gamma_2 = \frac{2\pi}{\lambda_0}\sqrt{(\frac{f_{c2}}{f})^2 - 1} \ . \tag{20}$$

Actually, this expression should have an additional term to account for the ohmic losses on the metal waveguide walls. Since this term is small relative to the cutoff decay a perturbation approach will be used.

The electric field expression for the lossless below-cutoff section is given by, Eq.21 where subscript t denotes the transmitted field.

$$E_{y2}=E_{t2}\sin\frac{\pi x}{a}e^{-\gamma_{z2}z} \tag{21}$$

Continuity of the tangential electric field across the boundary at z=0 requires that $E_{y1}=E_{y2}$ or,

$$E_{i1}\sin\frac{\pi x}{a}+\Gamma E_{i1}\sin\frac{\pi x}{a}=E_{t2}\sin\frac{\pi x}{a}\ . \tag{22}$$

Thus,

$$E_{t2}=E_{i1}(1+\Gamma)\ . \tag{23}$$

Using this equation in Eq.21 yields the expression for the electric field in the below cutoff region as,

$$E_{y2}=E_{i1}(1+\Gamma)\sin\frac{\pi x}{a}e^{-\gamma_{z2}z}\ . \tag{24}$$

The magnetic field expressions are obtained by applying the same method that was used in region 1. This yields,

$$H_{x2}=-\frac{j}{w\mu}\frac{\partial E_{y2}}{\partial x} \tag{25}$$

$$H_{z2}=\frac{j}{w\mu}\frac{\partial E_{y2}}{\partial x}\ . \tag{26}$$

Substituting Eq.24 into Eq.25 and Eq.26, the expressions for the transverse and longitudinal magnetic fields are obtained as

$$H_{z2}=\frac{j}{w\mu}k_x E_{11}(1+\Gamma)\cos\frac{\pi x}{a}e^{-\gamma_2 z} \tag{27}$$

$$H_{x2}=j\frac{\gamma_2}{w\mu}E_{11}(1+\Gamma)\sin\frac{\pi x}{a}e^{-\gamma_2 z} \tag{28}$$

D. TOTAL POWER LOSS IN THE BELOW-CUTOFF REGION

1. A discussion on the skin effect, surface currents, surface resistance, and power loss

Good conductors such as metals can be characterized by their very low intrinsic impedance and high attenuation, hence an electromagnetic wave is attenuated very rapidly in a metal medium as it attempts to propagate. The penetration depth in which the electromagnetic wave decays to 1/e (37 %) of its initial surface value is defined as skin depth, δ_s . In this manner, the currents induced by the propagating fields associated with the waveguide mode, flow in the inner surface layer of the metallic waveguide walls due to the skin effect and are treated as surface currents.

Surface currents on the waveguide walls are induced by the tangential magnetic field components of the electromagnetic wave and are given by,

$$\overline{J_s}=\overline{n}\times\overline{H_t} \tag{29}$$

where n is the unit vector normal to the metallic wall and pointed toward the inside of the waveguide.

In practice, the assumption of perfectly conducting metal walls is not true. Finite conductivity of the metal walls causes ohmic losses which results in the attenuation of the electromagnetic wave. Assuming that the wall currents are uniformly distributed over a thickness of one skin depth, the resistance applied to the current flow across the cross-sectional area of one-unit-square of the inner layer of the waveguide walls can be defined as surface resistance and is given by,

$$R_s = \frac{1}{\sigma \delta_s} \tag{30}$$

where σ and δ_s represents the conductivity and the skin depth of the material respectively.

Power loss for a waveguide wall is obtained by evaluating the integral below,

$$P_{walls} = \frac{1}{2}\int_s \int R_s |\bar{J}_s|^2 da \tag{31}$$

in this expression the product of the magnitude square of the current density with surface resistance represents the power dissipated per unit area at a point on the waveguide wall. The surface integral of this product over the total wall area gives the total power loss in the wall. The concepts that were discussed in this section are demonstrated in Fig.6.

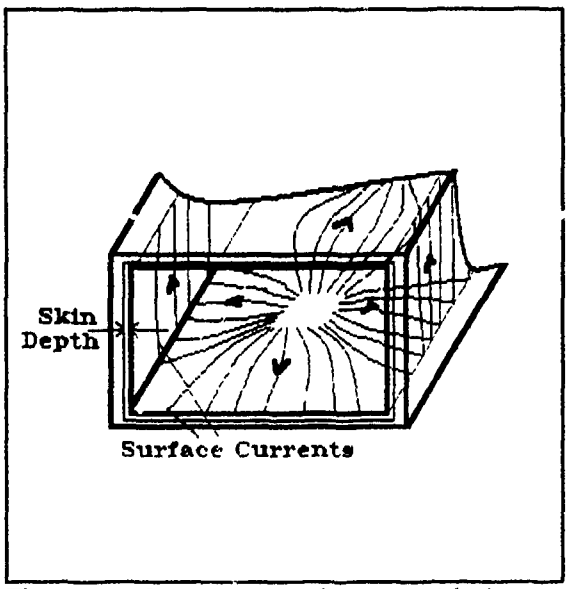

Figure 6. Cross-sectional waveguide layout shows the current flows.

2. Surface currents induced in the below-cutoff region

Surface currents, that are induced in the below cut-off region by the tangential magnetic field components of the TE_{10} evanescent mode, are obtained for each wall by utilizing Eq.29. Fig.7 illustrates the unit vectors normal to the waveguide walls in the cross-sectional plane.

a. *Top Wall*

The transverse and the longitudinal magnetic field components are both tangential to the top wall, hence the corresponding surface currents flow in both transverse and longitudinal directions on the top wall where y=b and $\overline{n}=-\overline{a_y}$.

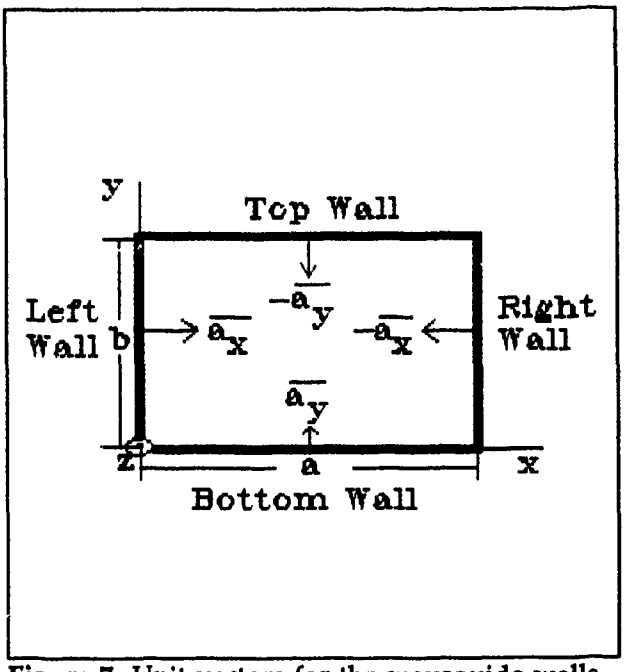

Figure 7 Unit vectors for the waveguide walls

Rewriting Eq.29,

$$\overline{J_{s_T}}=-\overline{a_y}\times[H_{x2}(x,b,z)\overline{a_x}+H_{z2}(x,b,z)\overline{a_z}] \tag{32}$$

and substituting Eq.27 and Eq.28 into Eq.32 yields the expression for the induced surface current density on the top wall.

$$\overline{J_{s_T}}=E_{11}(1+\Gamma)[(\frac{j\gamma_2}{\omega\mu})\sin\frac{\pi x}{a}\overline{a_z}-(\frac{jk_x}{\omega\mu})\cos\frac{\pi x}{a}\overline{a_x}]e^{-\gamma_2 z} \tag{33}$$

b. **Bottom Wall**

Like the top wall, the transverse and the longitudinal magnetic fields are tangential to the bottom wall where the normal unit vector points in the opposite direction. This indicates the same magnitude but the reverse direction surface current flows on the bottom wall with respect to the top wall. Substituting the values of y=b and $\overline{n}=\overline{a_y}$ into Eq.29,

$$\overline{J_{s_B}}=+\overline{a_y}\times[H_{x2}(x,b,z)\overline{a_x}+H_{z2}(x,b,z)\overline{a_z}] \quad . \tag{34}$$

Comparing Eq.34 with Eq.32 yields,

$$\overline{J_{s_B}}=-\overline{J_{s_T}} \quad . \tag{35}$$

c. **Left Wall**

Since the discontinuity of the perpendicular magnetic fields on the conductors requires the magnitude of the transverse magnetic field to be zero on the left wall (x=0, $\overline{n}=\overline{a_x}$), the surface current on this wall is induced only by the longitudinal magnetic field and flows in the transverse direction. The surface current density for the left wall is obtained by using Eq.29,

$$\overline{J_{s_L}}=\overline{a_x}\times H_{z2}(0,y,z)\overline{a_z} \tag{36}$$

and utilizing the magnetic field expression in Eq.36

$$\overline{J_{s_L}}=-\frac{jk_x}{w\mu}E_{11}(1+\Gamma)e^{-\gamma_2 z}\overline{a_y} \quad . \tag{37}$$

*d. **Right Wall***

The surface currents on the right and left walls are equal in magnitude and flow in the same direction. Using (x=a, $\overline{n}=-\overline{a_x}$) Eq.29,

$$\overline{J_{s_R}}=-\overline{a_x}\times H_{z2}(a,y,z)\overline{a_z} . \tag{38}$$

Comparison of Eq.38 and Eq.36 gives

$$\overline{J_{s_R}}=\overline{J_{s_L}} . \tag{39}$$

3. Power loss in the below-cutoff region

As discussed before, power is dissipated in the below cut-off section because of the ohmic losses. In order to determine the power dissipated on the waveguide walls due to the finite resistivity of the walls, it is assumed that the derived field expressions accurately describe the electromagnetic wave in the below-cutoff region. The power loss on each wall is obtained by using the associated current density expression in Eq.31.

*a. **Top & Bottom Walls***

The magnitude square of the surface current density for top & bottom the walls is given by

$$|J_s|^2=(\frac{\gamma_2}{w\mu})^2E_{11}{}^2|1+\Gamma|^2\sin^2\frac{\pi x}{a}e^{-2\gamma_2 z}+(\frac{k_x}{w\mu})^2E_{11}{}^2|1+\Gamma|^2\cos^2\frac{\pi x}{a}e^{-2\gamma_2 z} . \tag{40}$$

This expression is identical for both of the walls, and indicates that the same amount of power is dissipated on each wall.

Substituting Eq.40 into Eq.31 yields

$$P_{T,B}=R_sE_{11}^2|1+\Gamma|^2\int_0^a\int_0^\infty[(\frac{\gamma_2}{\omega\mu})^2\sin^2\frac{\pi x}{a}+(\frac{k_x}{\omega\mu})^2\cos^2\frac{\pi x}{a}]e^{-2\gamma_2 z}\,dxdz . \tag{41}$$

Carrying out the integral over bottom/top wall area that extends to $z=\infty$ due to the semi-infinite structure and doubling the result gives the expression for the total power loss on the top and the bottom walls

$$P_{T,B}=R_s E_{11}^2 |1+\Gamma|_2 [(\frac{\gamma_2}{\omega\mu})^2 \frac{a}{2}\frac{1}{2\gamma_2}+(\frac{k_x}{\omega\mu})^2 \frac{a}{2}\frac{1}{2\gamma_2}] \tag{42}$$

Equation 42 can be rewritten as,

$$P_{T,B}=\frac{R_s E_{11}^2 |1+\Gamma|^2}{4\gamma_2 a}[(\frac{\gamma_2 a}{w\mu})^2+(\frac{k_x a}{w\mu})^2] \, . \tag{43}$$

b. Left & Right Walls

Power is similarly dissipated on the left and right walls. The expression for the total power loss on these walls is obtained by using the same procedure as above with the required current density expression and integral limits as follows:

$$|J_s|^2=(\frac{k_x}{w\mu})^2 E_{11}^2 |1+\Gamma|^2 e^{-\gamma_2 z} \tag{44}$$

$$P_{L,R}=\frac{1}{2}\int_0^b\int_0^\infty R_s (\frac{k_x a}{w\mu})^2 E_{11}^2 |1+\Gamma|^2 e^{-2\gamma_2 z} dydz \tag{45}$$

$$P_{L,R}=R_s (\frac{k_x a}{w\mu})^2 E_{11}^2 |1+\Gamma|^2 \frac{2b}{a}(\frac{1}{4\gamma_2 a}) \, . \tag{46}$$

c. Total Power Loss

The summation of the results obtained in subsections a and b gives the total power loss, and it can be expressed as, $P_{2(walls)} = P_{(top\&bottom)} + P_{(left\&right)}$ which is the total amount of the

power dissipated on each wall in the below-cutoff region. The substitution of the associated loss expressions gives,

$$P_{2_{walls}}=\frac{R_s E_{11}^2|1+\Gamma|^2}{4\gamma_2 a}[(\frac{\gamma_2 a}{w\mu})^2+(\frac{k_x a}{w\mu})^2]+\frac{R_s E_{11}^2|1+\Gamma|^2}{4\gamma_2 a}[\frac{2b}{a}(\frac{k_x a}{w\mu})^2] \quad (47)$$

This equation can be rewritten as,

$$P_{2_{walls}}=\frac{R_s E_{11}^2|1+\Gamma|^2}{4\gamma_2 a}[(\frac{\gamma_2 a}{w\mu})+(\frac{k_x a}{w\mu})(1+\frac{2b}{a})] \quad (48)$$

and finally the expression for the total power dissipated due to ohmic losses in the below cutoff section is obtained as,

$$P_{2_{walls}}=\frac{R_2 E_{11}^2|1+\Gamma|^2(\gamma_2 a)}{4(w\mu)^2}[1+(\frac{k_x a}{\gamma_2 a})^2(1+\frac{2b}{a})] \quad (49)$$

III. DERIVATION OF THE QUALITY FACTOR FOR THE CUTOFF SECTION

In this chapter energy considerations, Q factor, and the characteristic impedance for a below-cutoff section will be discussed. The power loss for a finite length of below-cutoff waveguide will be utilized in terms of finite Q and the resistive part of the characteristic impedance.

A. ENERGY CONSIDERATIONS IN THE BELOW CUTOFF REGION

In the previous chapter the field expressions and the power loss due to the ohmic effect were derived for the non-propagating, below cutoff section.

In order to set up evanescent modes, the waveguide structure shown in Figure 8 was employed. This method avoids a change in the waveguide cross-section at the junction between the dielectric loaded propagating region and the air filled cutoff region.

Inspection of the structure for TE_{10} dominant mode propagation shows that in the first region the waveguide width is greater than the dielectric half wavelength,

$$a > \frac{\lambda_d}{2}.$$

Hence, the structure supports electromagnetic wave propagation and power flow. In the second region the waveguide width is less than the free-space half wavelength,

$$a < \frac{\lambda_o}{2}$$

thus the waveguide structure doesn't support electromagnetic wave propagation.

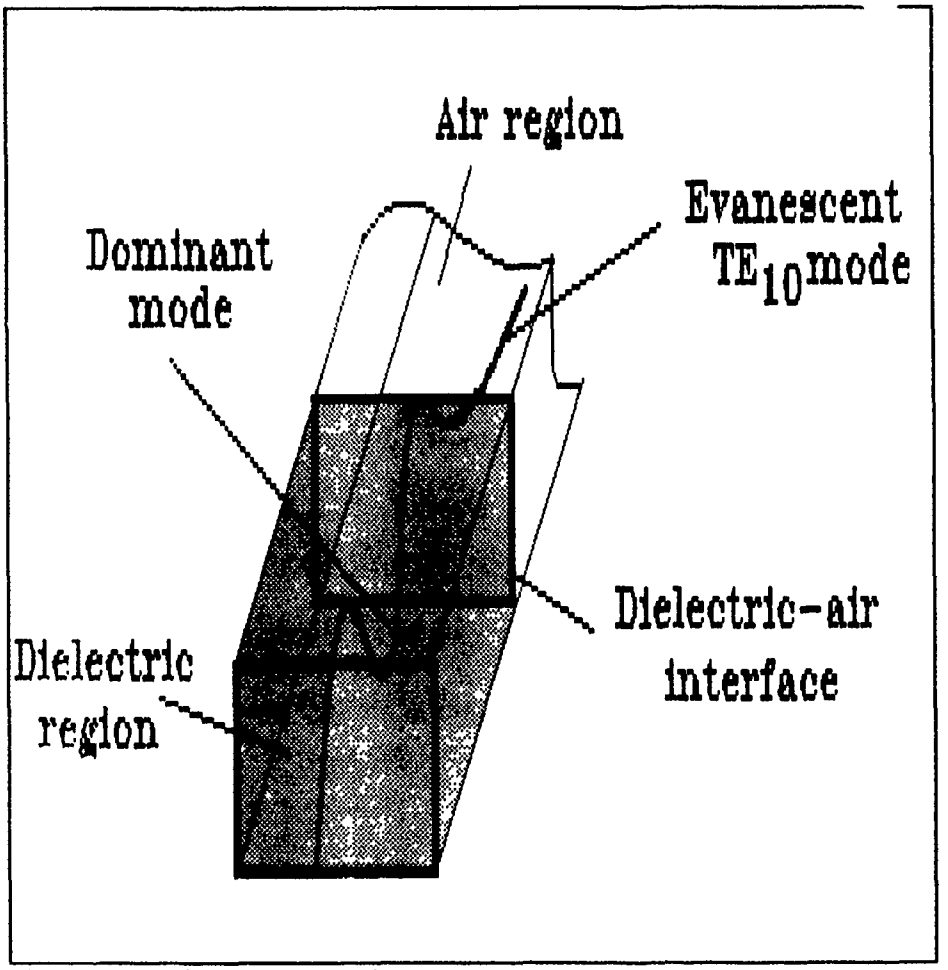

Figure 8. Dielectric-air interface.

Under the assumption of an excited dominant mode in the structure given in Figure 8, the TE_{10} electromagnetic wave propagates down to the junction where the further propagation of the wave is not supported by the air section.

In the lossy structure , at the dielectric-air interface, the dominant mode is reflected with a reflection coefficient less than unity. The transmitted part of the dominant TE_{10} mode creates the

evanescent TE_{10} mode in the air section. Thus, in the vicinity of the interface, the field can be represented by non-propagating (the propagation is not supported in this region) TE_{10} mode, with amplitude which decays as a function of distance from the dielectric-air interface and an attenuation constant given in Eq.20. Since the evanescent TE_{10} mode is attenuated as a function of distance from the interface, it is confined to a region near the air-dielectric interface. Referring to the below-cutoff field equations given in Eq.24-26, it can be observed that for a lossless guide the electric and magnetic fields are 90 degrees out of phase which means that no real power flow occurs in the below-cutoff region. Thus, no power is transmitted. The energy flux or the power calculated by the Poynting vector is purely imaginary.

The presence of the confined evanescent modes that are near the interface can be analyzed in terms of the stored energy since the localized fields represent stored magnetic and electric energy. Further investigation shows that the energy is predominantly stored in magnetic field, hence the existence of evanescent TE_{m0} modes can be represented by stored magnetic energy.

B. DERIVATION OF STORED MAGNETIC AND ELECTRIC ENERGY IN THE BELOW-CUTOFF REGION

1. Stored Electric Energy

In general, the peak stored energy may be obtained by integrating $\frac{1}{2}\epsilon_0|E|^2$ over the volume desired, that is,

$$U_e=\frac{1}{2}\int_v \bar{D}.\bar{E}dv=\frac{1}{2}\epsilon\int_v |\bar{E}|^2 dv \ . \qquad (50)$$

The peak stored electric energy in a cutoff section of length l is obtained by employing the evanescent TE_{10} mode electric field expression (Eq.24), in the equation given above, this yields,

$$U_e=\frac{1}{2}\epsilon\int_v |E_{y2}|^2 dv \ . \qquad (51)$$

Substituting integral limits gives,

$$U_e=\frac{1}{2}\epsilon\int_0^l\int_0^b\int_0^a E_{11}^2|1+\Gamma|^2\sin^2\frac{\pi x}{a}e^{-\gamma_2 z}\,dxdydz. \qquad (52)$$

The evaluation of the integral over the cutoff section volume renders the expression for the peak stored electric energy as,

$$U_e=\frac{1}{2}\epsilon E_{11}^2|1+\Gamma|^2\frac{a}{2}b\frac{1}{2\gamma_2}(1-e^{-2\gamma_2 l}) \ . \qquad (53)$$

This expression can finally be written as,

$$U_e=\frac{ab}{8\gamma_2}\epsilon E_{11}^2|1+\Gamma|^2(1-e^{-2\gamma_2 l}) \ . \qquad (54)$$

2. Stored Magnetic Energy

Stored magnetic energy in a volume is given by the integral,

$$U_m=\frac{1}{2}\int_v \bar{B}.\bar{H}dv=\frac{1}{2}\int_v \mu.|H|^2 dv \qquad (55)$$

and substitution of the transverse and the longitudinal below cutoff magnetic field expressions yields,

$$U_m=\frac{1}{2}\int_{v}\mu|H_{x2}|^2dv+\frac{1}{2}\int_{v}\mu|H_{z2}|^2dv \tag{56}$$

and,

$$U_m=\frac{1}{2}\int_0^l\int_0^b\int_0^a\mu(\frac{k_x}{\omega\mu})^2E_{il}^2|1+\Gamma|^2\cos^2\frac{\pi x}{a}e^{-2\gamma_2 z}dxdydz$$

$$+\frac{1}{2}\int_0^l\int_0^b\int_0^a\mu(\frac{\gamma}{\omega\mu})^2E_{il}^2|1+\Gamma|^2\sin\frac{\pi x}{a}e^{-2\gamma_2 z}dxdydz\ . \tag{57}$$

The evaluation of the integral over the cutoff volume results in the stored peak magnetic energy expression as

$$U_m=\frac{1}{2}\mu(\frac{k_x}{\omega\mu})^2E_{il}^2|1+\Gamma|^2\frac{a}{2}b\frac{1}{2\gamma_2}(1-e^{-2\gamma_2 l})$$

$$+\frac{1}{2}\mu(\frac{\gamma_2}{\omega\mu})^2E_{il}^2|1+\Gamma|^2\frac{a}{2}b\frac{1}{2\gamma_2}(1-e^{-2\gamma_2 l})\ . \tag{58}$$

This can be rewritten as

$$U_m=\frac{ab}{8\gamma_2}E_{il}^2|1+\Gamma|^2\frac{1}{\omega^2\mu}(k_x^2+\gamma_2^2)(1-e^{-2\gamma_2 l})\ . \tag{59}$$

Substituting the expression, $k_x^2=\gamma^2+\omega^2\mu\epsilon$ yields,

$$U_m=\frac{ab}{8\gamma_2}E_{il}^2|1+\Gamma|^2\frac{1}{\omega^2\mu}(\gamma_2^2+\gamma_2^2+\omega^2\mu\epsilon)(1-e^{-2\gamma_2 l})\ . \tag{60}$$

which can be rewritten as

$$U_m=\frac{ab}{8\gamma_2}E_{il}^2|1+\Gamma|^2\epsilon(\frac{2\gamma_2^2}{\omega^2\mu\epsilon}+1)(1-e^{-2\gamma_2 l})\ . \tag{61}$$

Inspection of the stored electric and magnetic energy expressions shows that the maximum stored energy in the below cutoff region always occurs predominantly in the magnetic field, since $(\gamma_2 / \omega\sqrt{\mu\varepsilon})>1$.. The amount of the energy stored in both fields is frequency dependent. As the operating frequency decreases below the cutoff frequency, the stored energy increases in magnetic field and decreases in electric field. The energy in the fields is equal at the cutoff frequency. This result is easily observed from the ratio of the stored magnetic and electric energies,

$$\frac{U_m}{U_e}=\frac{\frac{ab}{8\gamma_2}E_{11}^2|1+\Gamma|^2\varepsilon(\frac{2\gamma_2}{\omega^2\mu\varepsilon}+1)(1-e^{-2\gamma_2 l})}{\frac{ab}{8\gamma_2}\varepsilon E_{11}^2|1+\Gamma|^2(1-e^{-2\gamma_2 l})} \tag{62}$$

$$\frac{U_m}{U_e}=\frac{2\gamma_2}{\omega_2\mu\varepsilon}+1 \; . \tag{63}$$

Substituting the definition of the propagation factor (Eq.20) yields

$$\frac{U_m}{U_e}=2(\frac{f_{c2}}{f})^2-1 \; . \tag{64}$$

In the expression above, the decrease in the operating frequency, f, causes an increase in the energy ratio which illustrates that the amount of energy stored shifts from electric to magnetic. This is a useful result that will be utilized in the further modelling concept of the below cutoff section.

C. DERIVATION OF THE QUALITY FACTOR FOR THE BELOW-CUTOFF WAVEGUIDE SECTION

Unless the waveguide is lossless, stored energy is dissipated due to the finite conductivity of the guide walls which introduces ohmic losses. The Quality Factor for a guide excited in the TE_{10} evanescent mode can be defined on the basis of stored energy / dissipated energy. The Q factor is finite rather than infinite as it would be in the lossless case.

The definition of the Q factor may be given by,

$$Q=2\pi\frac{\textit{Maximum Stored Energy}}{\textit{Energy Dissipated}} \tag{65}$$

where the energy dissipated is equivalent to the power dissipated per unit bandwidth which yields,

$$Q=\omega\frac{\textit{Maximum Stored Energy}}{\textit{Power Dissipated}} . \tag{66}$$

As stated in the previous section, the maximum stored energy occurs in the magnetic field, so the Q factor for the below cutoff waveguide is

$$Q=\omega\frac{\textit{Peak Stored Magnetic Energy}}{\textit{Power Loss}} \tag{67}$$

or,

$$Q=\omega\frac{U_m}{P_w} . \tag{68}$$

In chapter II, section B, the expression for power loss was derived for a semi-infinite, below-cutoff guide. In order to obtain the power loss for a cutoff guide of length 'l', the same

definition of power loss (Eq.30) can be used. Integrating over a finite length, l, yields,

$$P_w=\frac{R_s}{4\gamma_2 a}E_{11}^2|1+\Gamma|^2[(\frac{\gamma_2 a}{\omega\mu})^2+\frac{k_x a}{\omega\mu})^2(1+\frac{2b}{a})](1-e^{-2\gamma_2 l}) . \tag{69}$$

Substituting Eq.69, Eq.61 into Eq.67 gives

$$Q=\omega\frac{\frac{ab}{8\gamma_2}E_{11}^2|1+\Gamma|^2\frac{1}{\omega^2\mu}(k_x^2+\gamma_2^2)(1-e^{-2\gamma_2 l})}{\frac{R_s}{4\gamma_2 a}E_{11}^2|1+\Gamma|^2[(\frac{\gamma_2 a}{\omega\mu})^2+(\frac{k_x a}{\omega\mu})^2(1+\frac{2b}{a})](1-e^{-2\gamma_2 l})} \tag{70}$$

which can be rewritten as,

$$Q=\omega\mu\frac{\frac{ab}{8\gamma_2}(k_x^2+\gamma_2^2)}{\frac{R_s}{4\gamma_2}[a(\gamma_2^2+k_x^2)+2bk_x^2]} . \tag{71}$$

The definition of the Q factc for the below-cutoff waveguide is obtained as,

$$Q=\frac{\omega\mu}{R_s}\frac{ab}{2}\frac{[1+(\frac{\gamma_2}{k_x})^2]}{a[1+(\frac{\gamma_2}{k_x})^2]+2b} \tag{72}$$

which is equivalent to the definition given on page 307 of Ref.8. Substituting the expression,

$$(\frac{\gamma_2}{k_x})^2=\frac{\omega^2\mu\epsilon[(\frac{f_c}{f})^2-1]}{\omega^2\mu\epsilon(\frac{f_c}{f})^2}=1-(\frac{f}{f_c})^2 \tag{73}$$

into Eq.72 yields,

$$Q=\frac{\omega\mu}{R_s}\frac{ab}{2}\frac{[1-\frac{1}{2}(\frac{f}{f_c})^2]}{a[1-\frac{1}{2}(\frac{f}{f_c})^2]+b} \quad (74)$$

As observed from the result given in Eq.74, the Q expression is a general definition. It is independent of the dielectric constant of the region 1 (Fig.5) and can be used for any evanescent waveguide. It is also independent of the guide length. This can be explained in terms of the volume to surface area ratio where the energy is stored and dissipated respectively. For a below-cutoff guide, the ratio of volume to surface area is given by,

$$\frac{Volume}{Surface\ Area}=\frac{abl}{2(a+b)l}=\frac{ab}{2(a+b)} \quad (75)$$

a change in the waveguide length effects the volume and the surface area in the same proportion. Thus, the variation of the Q factor with the volume-to-surface area is independent of the guide length, but dependent on the cross-section. Therefore, it can be concluded that the Q factor is constant for any length of the below-cutoff waveguide at a particular frequency. This gives insight for the modeling concept.

D. THE RESISTIVE PART OF THE CHARACTERISTIC IMPEDANCE

The characteristic impedance of a lossless below-cutoff waveguide is a pure inductive reactance (Eq.4). Above-cutoff,

waveguide can be visualized as a two wire structure shunted by an array of quarterwave shorted stubs ($l=\lambda/4$) [Ref.9]. Since the admittance of the stubs is zero energy propagates down the guide without loss (Fig.9). The same configuration can be used for a below-cutoff guide except that the length of the stubs is less than a quarter wavelength ($l<\lambda/4$). Thus, the stub input impedance is inductive.

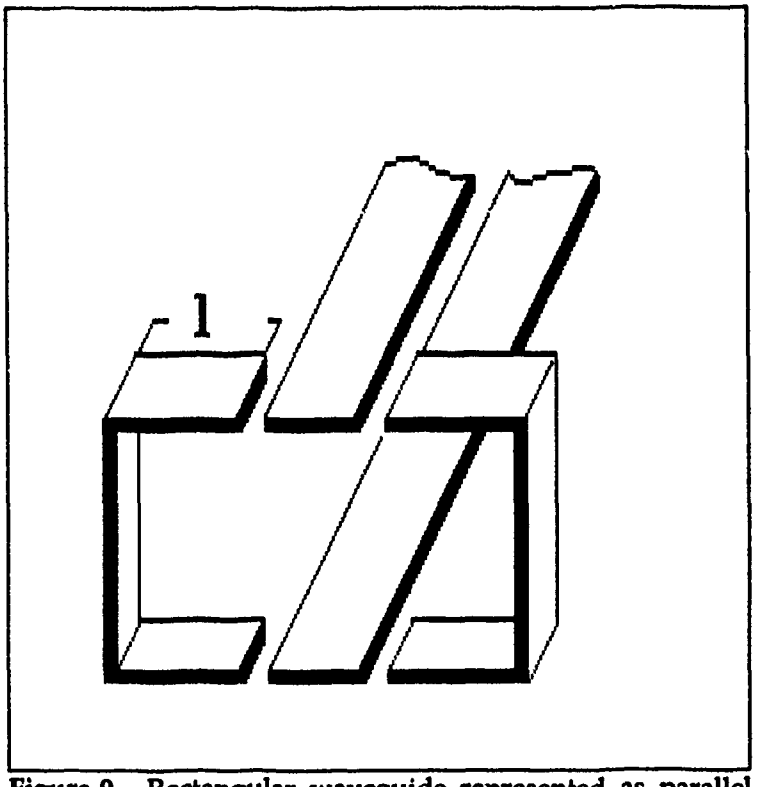

Figure 9. Rectangular waveguide represented as parallel plate transmission line and quarter-wave shorted stubs.

In the case where the conductive losses are also included, the characteristic impedance is complex and consists of inductance with a series resistance that accounts for the dissipative losses on the guide walls. Thus the semi-infinite, below-cutoff part of the structure given in figure 5 can be replaced with an equivalent load impedance $Z_{02}=R_{02}+jX_{02}$.

The expression for R_{02} can be found from the definition of Q,

$$Q=\frac{\omega L}{R}=\frac{X_{02}}{R_{02}} \tag{76}$$

and,

$$R_{02} \approx \frac{X_{02}}{Q} \tag{77}$$

substituting Eq.4 and Eq.72 into Eq.77 yields,

$$R_{02} = \frac{2R_s}{b} \frac{\gamma_2}{(k_x^2 + \gamma_2^2)} [1 + (\frac{k_x}{\gamma_2})^2 (1 + \frac{2b}{a})] \tag{78}$$

IV. INDUCTIVE STRIP LEADING EDGE LOSS

As a lossy finline discontinuity, the inductive strip causes dissipation of power. In the previous chapters associated wall losses were evaluated and related expressions were developed. In this chapter the edge losses of the strip will be analyzed.

A. STRIP EDGE DISCONTINUITY EFFECT

A configuration of the inductive strip in homogeneous finline is given in the Figure 2. It is an obstacle in the finline structure that interrupts the electromagnetic wave propagation and creates a finline discontinuity. The discontinuity effect of the strip may be well analyzed in the structure given in Figure 10 where the strip with thickness t and length T is shown centered in a homogeneous finline structure that has zero fin heights.

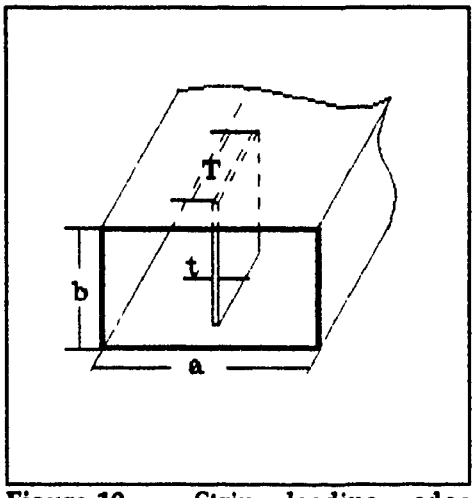

Figure 10. Strip leading edge discontinuity in a zero fin height finline structure.

Hence the strip is centered in the finline and the configuration is symmetric over the center line that connects the broad sides. Typically, thickness is only a very small fraction of the guide width. Under these circumstances, only the propagation of the odd numbered TE_{m0} modes are interrupted by the leading edge, whereas, the even numbered modes propagate

without being interrupted, because for these modes E_y=0 on the centerline where the strip is located.

Inspection of Figure 10 shows that the leading edge with thickness t spans a rectangular area in the transverse plane on the centerline; breaks the continuity of the broad edge of the waveguide hence becomes an H plane discontinuity. The necessity of satisfying boundary conditions at a discontinuity requires the presence of the higher order modes which account for the discontinuity effect.

As a discontinuity, the leading edge of the strip generates higher-order TE modes around the edge. Since the physical dimensions of the sections located on either side of the strip are not sufficient to support any waveguide propagation, the higher-order TE modes are attenuated in a short distance from the discontinuity. The localized TE modes represent stored magnetic energy, hence inductive effect.

The peak energy in the plane of discontinuity is directly proportional to the incident electric field at the edge and will be distributed over the dominant and higher order modes. Thus the total current flow on the edge can be find by using the model shown in Figure 11 and is equivalent to the summation of the higher order and dominant mode currents.

Therefore, the effect of the edge discontinuity can also be discussed from the circuit point of view by considering a total current that is conducted through the edge. Thus a magnetic flux will be produced that links the conduction current, creating an inductive effect.

As a result, the discontinuity effect of the strip leading edge can be represented by a shunt inductance assuming that the strip is lossless.

The amount of the total current linking through the edge is dependent on the finite conductivity of the strip, since it experiences a certain amount of resistance on the edge which causes dissipation of power. Thus, for the lossy case the edge discontinuity also shows a resistive effect in addition to the inductive effect, hence it can be modeled with finite Q inductor or a network consisting of resistive and inductive lumped elements.

B. AC ANALYSIS OF THE STRIP

The AC analysis of the inductive strip can be done from the circuit point of view. Considering the structure given in Figure 10 has been initially excited by an incident TE_{10} mode, it can be assumed that the distribution of the fields approximately uniform over the front end surface of the strip because of the very small thickness of the strip with respect to the width of the waveguide. The electric field in the reference plane of the discontinuity can be given by,

$$E_y = E_i(1+\Gamma)\sin\frac{\pi x}{a}e^{-\gamma z} \quad (79)$$

Thus, the value of the uniform electric field over the edge surface is obtained by evaluating the expression given in Eq.79 at x=a/2 and z=0 where the edge is located. It is,

$$E_e = E_i(1+\Gamma) \ . \tag{80}$$

From the circuit point of view this uniform, time dependent field can be replaced with an equivalent AC voltage source of the value,

$$V_e = bE_i(1+\Gamma) \ . \tag{81}$$

Since the edge discontinuity has resistive and inductive effects it can be visualized with an equivalent LR circuit given in Fig.11.

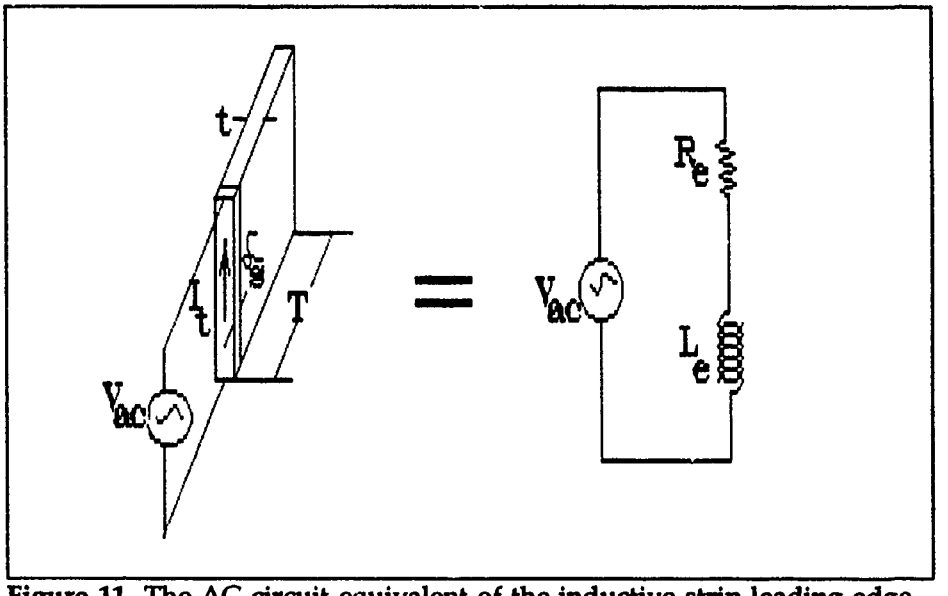

Figure 11 The AC circuit equivalent of the inductive strip leading edge.

The current flow in the circuit is equivalent to the total current which is the summation of the dominant and higher-order mode currents. The current density is function of z and is given by,

$$J_y = \sigma E_y e^{-\gamma z} = \sigma E_i(1+\Gamma)e^{-\gamma z} \ . \tag{82}$$

Thus, the total current is found by integrating the current density function over the cross-sectional area of the strip. It is,

$$I_T=\int_0^T\int_0^t J_y\,dx\,dz=\frac{\sigma}{\gamma}tE_i(1+\Gamma)(1-e^{-\gamma T}) \tag{83}$$

where the propagation factor in a good conductor is given by,

$$\gamma=\frac{1}{\delta_s}(1+j)\ . \tag{84}$$

And since $T>\delta_s$, the exponential term in Eq.84 can be assumed to be $e^{-\gamma T}=0$; hence the total current is,

$$I_T=\frac{\sigma\delta_s}{\sqrt{2}}tE_i(1+\Gamma)\ \angle -45 = \frac{1}{\sqrt{2}}\frac{t}{R_s}E_i(1+\Gamma)\ \angle -45\ . \tag{85}$$

The AC impedance of the strip can be obtained as,

$$Z_{AC}=\frac{V_{AC}}{I_T}=R_s\frac{b}{t}+jR_s\frac{b}{t}\ . \tag{86}$$

As long as the power loss is our concern the real part of this expression is important. Since the inductive effect of the higher order localized fields dominate, the imaginary part is insignificant. The AC resistance of the strip can be given by,

$$R_{AC}=R_s\frac{b}{t} \tag{87}$$

and is equivalent to the DC resistance of a rectangular bar of length b and transverse dimensions of δ_s and t. The value of the

resistance shown in Figure 11 is equivalent to the AC resistance of the strip given in Eq.87. Referring to the same figure, an equivalent expression for the inductance that accounts for the inductive effect of the strip leading edge can be found in the Thesis by Morua [Ref.10]. It is,

$$L=(\frac{b}{400})[A_1+(\frac{L_1}{L_2})] \tag{88}$$

and the coefficients are,

$$A_1=13.75-10.32(1-\frac{w}{b})^{1.6},$$

$$B_1=9.46-6.36(1-\frac{w}{b})^{3.78},$$

$$C_1=1.54-1.10(1-\frac{w}{b})^{4.73},$$

$$T_p=\frac{900T}{a},$$

$$N_1=500-241(1-\frac{w}{b})^{1.74},$$

$$L_1=B_1-C_1\ln(T_p),$$

$$L_2 1+e^{[(T-N_1)\frac{90}{a}]}$$

where w is the distance between the fins.

C. THE POWER LOSS AND STORED MAGNETIC ENERGY

The AC voltage source given in Figure 11 supplies energy to the circuit where some part of it is dissipated as heat energy on the resistance and the rest is stored in the inductance. Referring to the circuit the following equations can be written,

$$V=IR+L\frac{\partial I}{\partial t} \tag{89}$$

and,

$$VI=I^2R+LI\frac{\partial I}{\partial t}. \tag{90}$$

The term on the left side of the Eq.90 represents the rate at which the energy is supplied by the source; the first term on the right, I^2R, is the rate at which the energy is dissipated by the resistor and the second term on the right, $LI\frac{\partial I}{\partial t}$, is the rate at which the energy is stored into the inductance. The term I^2R can also be called the instantaneous power dissipated in the resistor. This power varies from zero to its maximum value RI^2_{max}. The average power dissipated in the resistor is given by,

$$P_{AV}=\frac{1}{2}|I_{max}|^2 Re|Z_{AC}|, \tag{91}$$

substituting the maximum current and the AC resistance yields,

$$P_e=\frac{1}{4}\frac{bt}{R_s}E_i^2|1+\Gamma|^2 . \tag{92}$$

This expression accounts for the average power loss on the edge which is dissipated by the resistance that dominant and the higher-order mode currents experience. The power dissipated on the edge is directly proportional with the strip thickness. This means that the thicker the strip, the more the power loss and vice versa. The stored magnetic energy in the inductance can be obtained from the second term on the right in Eq.90. It is,

$$\frac{\partial U_M}{\partial t}=LI\frac{\partial I}{\partial t}, \tag{93}$$

solving for stored magnetic energy ,UM, gives,

$$U_M=\frac{1}{2}L|I_{MAX}|^2 . \tag{94}$$

And substituting the maximum current expression yields the final expression for the stored magnetic energy in the inductance as,

$$U_M=\frac{1}{4}L\frac{t^2}{R_s^2}E_i^2|1+\Gamma|^2 . \tag{95}$$

Since the value of inductance L given in Figure 11 can be obtained from Eq.88 for any variation in the finline and strip dimensions, utilizing this value of L in Eq.95 accounts for the peak stored magnetic energy of the higher order modes in the vicinity of the strip edge.

D. THE QUALITY FACTOR OF THE EDGE

Quality factor of the circuit given in Figure 11 can be defined in terms of the stored and dissipated energy. It can be given as,

$$Q=\omega\frac{Stored\ energy}{Power\ loss} \tag{96}$$

and substituting the expressions for the stored energy (Eq.95) and power loss (Eq.92) yields,

$$Q=\omega\frac{\frac{1}{4}L\frac{t^2}{R_s^2}E_i^2|1+\Gamma|^2}{\frac{1}{4}b\frac{t}{R_s^2}E_i^2|1+\Gamma|^2}=\omega\frac{L}{R_s}\frac{t}{b} . \tag{97}$$

Inspection of the equation shows that,

$$Q=\omega\frac{L}{R_{AC}} , \tag{98}$$

which is the definition of Quality factor for series LR circuit.

Analysis of the power loss and the stored energy expressions indicates that the total current increases with the increasing thickness of the edge and with the higher conductivity of the strip. This increase in the total current flow increases the power loss and the stored energy both. But, with the increasing current flow more energy is stored in the inductance than is dissipated as heat on the resistance by a factor equal to the square root of the conductivity and the strip thickness, t. Thus the Q factor of the edge increases with the increasing strip thickness and conductivity. It can be deduced that the better the quality of the conductor that the strip is made of, and the thicker the strip is, the higher the Quality Factor of the strip edge discontinuity.

In the experiments that were conducted 2 mils thick beryllium copper was used as an inductive strip. Evaluation of the Q expression for this strip at 10 Ghz yields the value Q=45 which is quite different than the case where the edge inductance is assumed to be lossless with infinite Q. This shows that the finite conductivity of the strip has to be taken into account for the better prediction of the experimental results by the inductive strip circuit model.

V. MODEL CONCEPT

Until now, losses associated with the inductive strip were analyzed and related loss expressions were developed. In this chapter, the power loss will be included in the strip model and the improvement in the prediction of the experimental data will be inspected for a finline filter with and without loss.

A. APPLICATION OF BELOW CUTOFF LOSS TO THE FINLINE STRIP MODEL

Referring to the Figure 3, it was stated that the propagating dominant mode, and the higher order TE modes created by the edge discontinuity become evanescent in the below cutoff sections. These evanescent TE modes originate the localized fields hence are represented by stored magnetic energy. And, it was analytically shown that the more the operating frequency is below cutoff, the more the energy is stored in the magnetic field; from which it can be deduced that the below cutoff sections may be modelled by a reactive network that is made of inductive elements.

Generally a transmission line can be represented by an equivalent Tee circuit given in Figure 12. And the associated impedance matrix representations can be given by,

$$[Z]=\begin{bmatrix} Z_a+Z_c & Z_c \\ Z_c & Z_b+Z_c \end{bmatrix}=\begin{bmatrix} Z_0\coth(\gamma l) & \dfrac{Z_0}{\sinh(\gamma l)} \\ \dfrac{Z_0}{\sinh(\gamma l)} & Z_0\coth(\gamma l) \end{bmatrix} \tag{99}$$

Solving for the impedances yields,

$$Z_a=Z_b=Z_0[\coth(\gamma l)-\frac{1}{\sinh(\gamma l)}]=[\frac{\cosh(\gamma l)-1}{\sinh(\gamma l)}] \qquad (100)$$
$$Z_c=\frac{Z_0}{\sinh(\gamma l)}$$

where $[\frac{\cosh(\gamma l)-1}{\sinh(\gamma l)}]$ can be shown to be equivalent to $[\tanh(\frac{\gamma l}{2})]$. Thus the equivalent Tee impedances are,

$$Z_a=Z_b=Z_0\tanh(\frac{\gamma l}{2}) \qquad (101)$$
$$Z_c=Z_0 csch(\gamma l)$$

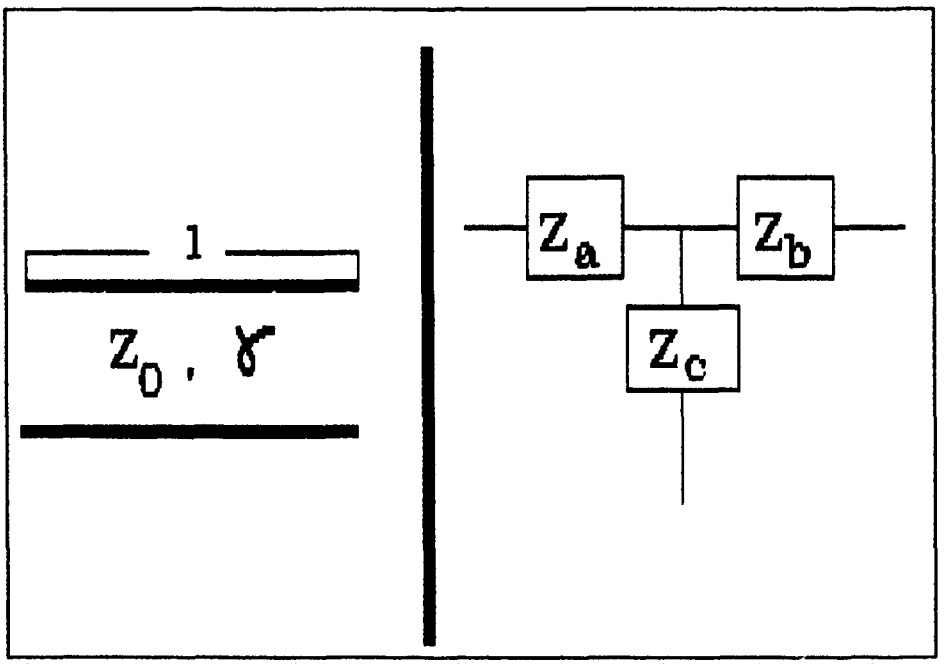

Figure 12 Tee equivalent circuit of a transmission line with length l.

A below-cutoff waveguide section may also be represented by an equivalent Tee circuit model. The model impedances are given by,

$$Z_a = Z_b = jX_0 \tanh\left(\frac{\gamma l}{2}\right)$$
$$Z_c = jX_0 \operatorname{csch}(\gamma l) \qquad (102)$$

where characteristic impedance X_0 is given by Eq.4.

Since the characteristic impedance of a lossless below-cutoff section is inductive, the Tee equivalent circuit model is composed of infinite Q, purely inductive elements emphasizing that the peak stored energy occurs in the magnetic field.

The model is dependent on the waveguide dimensions and operating frequency, but it is significantly sensitive to a variation in the guide length. A slight increase in the guide length, causes a small increase in Z_a and Z_b but a large decrease in Z_c that makes the middle branch closer to a short circuit. This means that the longer the below-cutoff guide is, the less the coupling becomes. And since the evanescent fields attenuate very rapidly with the distance, a better coupling can be maintained with the shorter below-cutoff guides which points out that the model is reasonable when the length of the guide is considered.

In Chapter III the resistive part of the characteristic impedance was developed associated with the wall losses.

Power loss can be included to the lossless model by making use of the characteristic impedance that accounts for the wall losses. It can be written as, $Z_0 = R_0 + jX_0$ where R_0 and X_0 are given by Eq.29 and Eq.4 respectively.

Thus impedances of the Tee circuit model for lossy below-cutoff waveguide may be given by,

$$Z_a=Z_b=(R_0+jX_0)\tanh(\frac{\gamma l}{2})$$
$$Z_c=(R_0+jX_0)csch(\gamma l) \quad (103)$$

and the model itself is given in Figure 13.

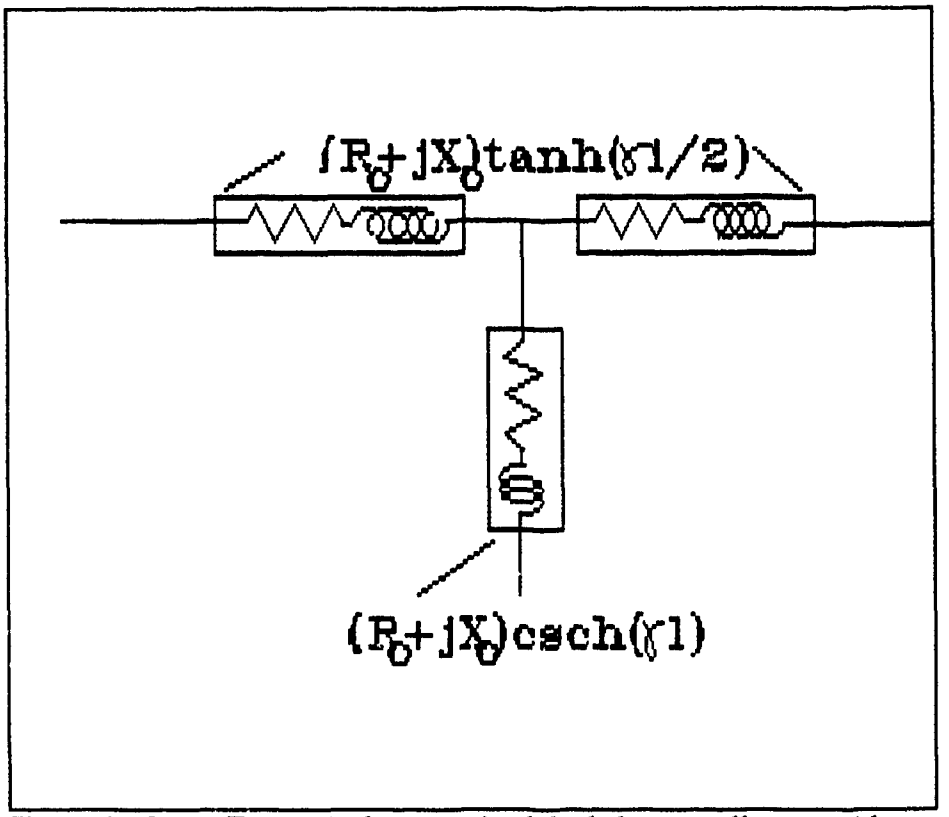

Figure 13 Lossy Tee equivalent circuit of the below-cutoff waveguide.

Another way of adding the effect of the power loss to the circuit model can be managed by replacing the dissipationless reactive elements with the dissipative ones; hence the infinite Q inductances can be replaced with the finite Q inductances. And since the Quality factor of a below-cutoff waveguide is independent of the guide length, using finite Q inductances can be considered as an equivalent approach to the one discussed above.

Referring to Figure 3, the below-cutoff waveguide sections can be replaced with a lossy Tee equivalent circuit model as shown in Figure 13.

Thus it is accomplished to include below-cutoff wall losses in the inductive strip circuit model.

B. APPLICATION OF EDGE LOSS TO THE FINLINE STRIP MODEL

In chapter IV, it was found that the strip edge has a resistance of R_e given in Eq.87.

To obtain an accurate response prediction for the inductive strip, the significant effect of the ohmic losses on the edge should be included in the lossless model. Referring to Figure 3, this can be performed by connecting the inductor in series with a resistance of the value equivalent to edge resistance, R_e. The other approach of using finite Q inductances as circuit element in the model is also valid for edge losses. This requires use of the Quality Factor derived for the inductive strip edge (Eq.98).

By including edge losses in the model, where the below-cutoff wall losses have already been included, it is possible to bring in all the associated losses to the CAD compatible circuit model of the inductive strip.

Three different lossless circuit models of inductive strip in homogeneous finline can be found in the technical report by Knorr [Ref.2]. These equivalent circuit models vary from simple to complex, and become more accurate with increasing complexity.

Figure 14 shows the lossy circuit model of the inductive strip. It is obtained by applying the associated losses to the most complex lossless model (Model 3) [page 11 in Ref.2].

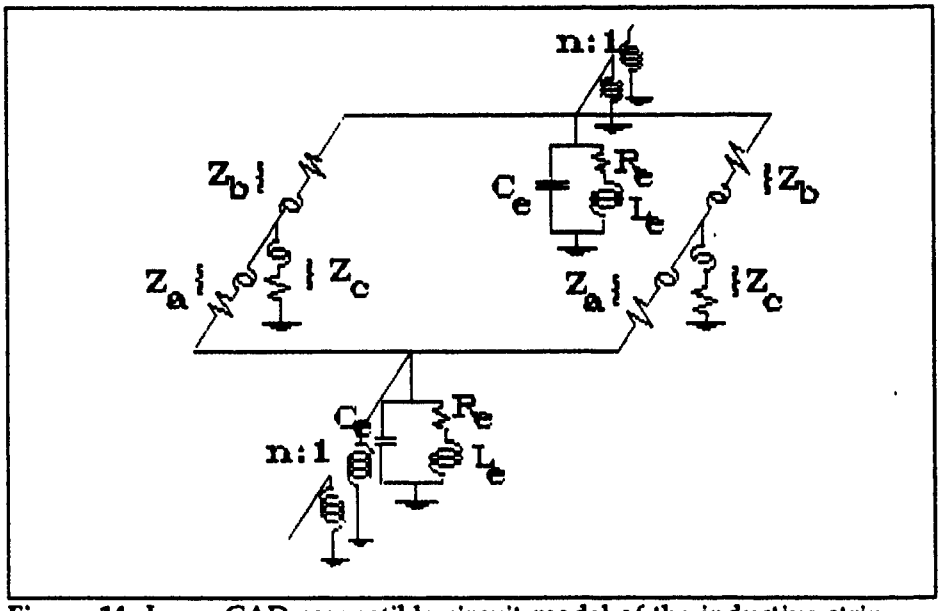

Figure 14 Lossy CAD compatible circuit model of the inductive strip.

C. COMPARISON OF THE EXPERIMENTAL AND THE CIRCUIT MODEL RESPONSE OF A FINLINE FILTER WITH AND WITHOUT LOSS

CAD compatible circuit model of the inductive strip in finline has wide application in designing networks with finline components. One of the principal applications of the model is designing finline filters.

Basically, a finline filter can be built by coupling high Q finline resonators together. And a finline resonator consist of two inductive strips separated by a length of finline where the strips are utilized as reflective boundaries.

An extensive study of finline resonators and filters can be found in Ref.2-6. One of the experiments that is discussed in Ref.6 is the measurement of the insertion and return loss of a symmetric X-band filter.

The filter configuration consists of 3 resonators and 4 strips with the dimensions (in mils) of T_1=90, R_1=558, T_2=250, R_2=540, T_3=240, R_3=540, T_4=90 where R and T represents the length of the resonator and the length of the strip respectively. And the fin structure of the filter is fabricated from a 2 mil thick sheet of beryllium copper that has a conductivity 25 % that of copper.

The response of the filter was measured on HP8756 scalar network analyzer. It consists of insertion and return loss curves. The response that is taken from Ref.6 is given in Fig.15.

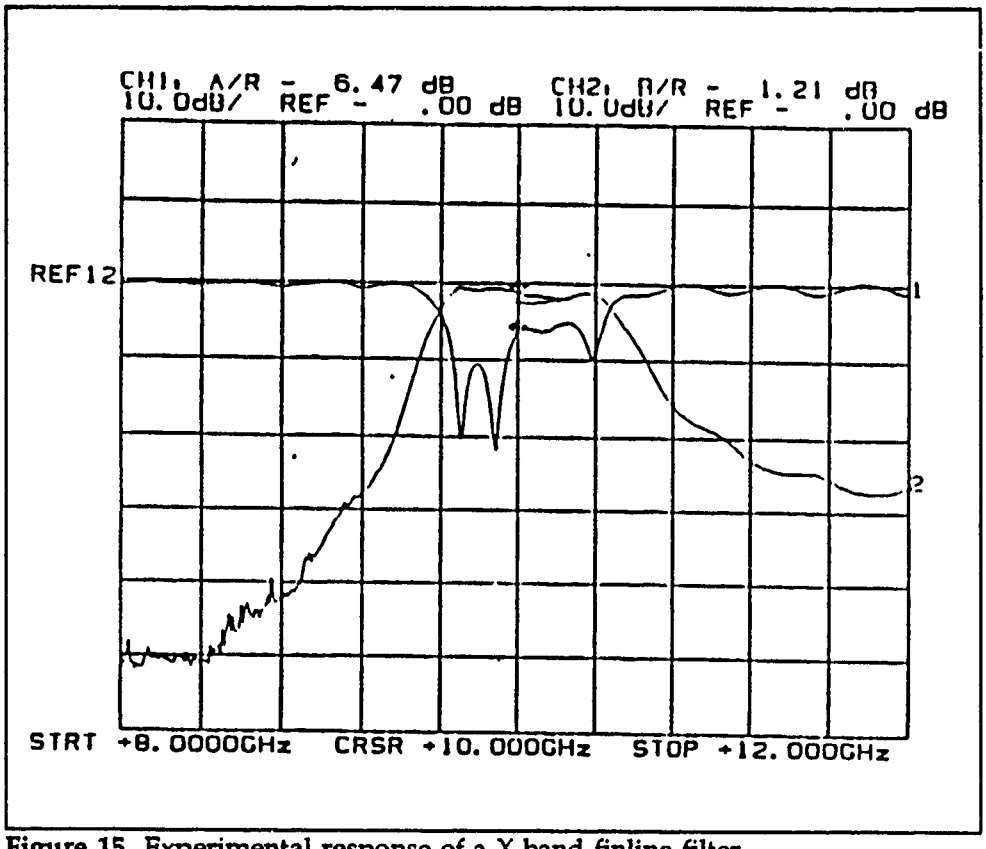

Figure 15 Experimental response of a X-band finline filter

The same X-band filter was modeled by using the circuit model of the strip with and without loss. The predicted response using

by both lossy and lossless models were compared with the experimental response to evaluate the discrepancy created by the loss.

Touchstone software was used to simulate the filter and to obtain the predicted response. The lossy model of the strip was constructed using finite Q inductors as the only circuit element. This approach results in the same predicted response as using series resistances would, but it is simpler.

The loss associated with the resonator gaps is accounted for the software since they are defined by the equivalent waveguide sections. Another loss source associated with the experimental response of the filter is due to housing (shield) in which the filter structure is placed and measurements are taken. Extra length of the shield creates additional losses. These losses were also included in the model by connecting the necessary lengths of finline to both ends of the filter circuitry.

Thus, the equivalent circuit model of the X-band finline filter would be able to account for all the associated losses. The circuit and the data file is given in Appendix A.

The predicted response of the filter was obtained in the same frequency band as the experimental response to ease point by point comparison. It was plotted on the same grid for the lossy and lossless models and is presented in Figure 16.

First, the predicted response without loss was compared with the experimental response. It can be seen that both the insertion and return loss curves are in very good agreement.The two

significant discrepancies are in the pass band insertion and the return loss. The measured insertion loss varies between 1 and 2.5

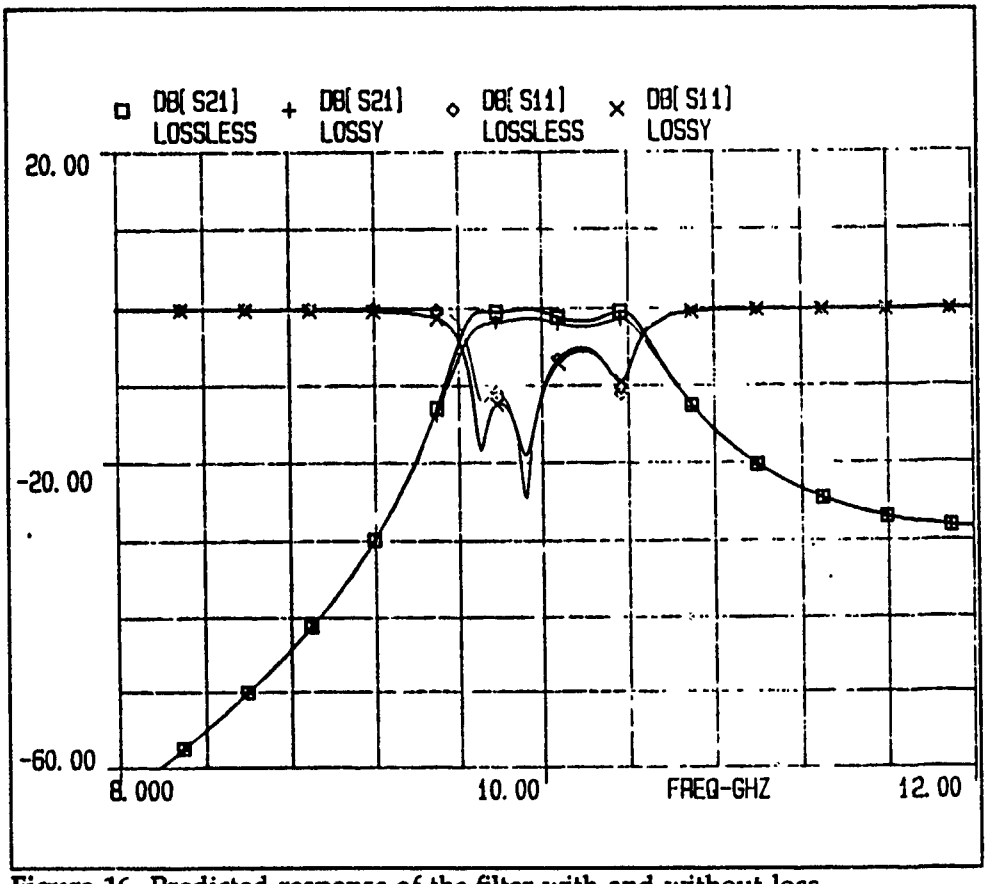

Figure 16 Predicted response of the filter with and without loss.

db which is small but remarkably greater than the predicted insertion loss. There are small but noticeable differences between the shape of the experimental and predicted return loss curves which shows a maximum difference of 6 db.

Point by point comparison of the experimental response and the predicted response with loss, shows that the insertion and return loss curves are in even better agreement than the previous lossless case. Both of the discrepancies found in the lossless case are reduced in the predicted response of the lossy model.

The predicted insertion and return losses are almost equivalent to those measured, with maximum difference of 1 db.

Thus, it can be deduced that a significant improvement is obtained in the accuracy of the predicted response of the filter by utilizing the lossy circuit model of the inductive strip.

VI. CONCLUSIONS AND RECOMMENDATIONS

A. CONCLUSIONS

This thesis describes the derivation of the analytical loss expressions for the inductive strip septum in homogeneous finline and the inclusion of the loss in the equivalent circuit model. The losses associated with the inductive strip were analyzed as ohmic losses, dissipated on the walls in below cutoff sections, and on the strip leading edge. Considering the energy flow through the inductive strip, it was analytically shown that both in the below-cutoff sections and around the strip leading edge, the energy is predominantly stored in magnetic field, justifying the inductive effect of the septum. The Quality Factors for both loss sources were derived by utilizing the Power Loss and Stored Energy expressions. Evaluation of the Q factors at 10 GHz results in the value of 5327 for below-cutoff sections and 45 for the strip leading edge. When compared with the below-cutoff wall losses, the significant role of leading edge loss on the overall strip losses can be recognized from the values of the Q factors.

Concerning the lossy model concept, the effect of the loss was included in the circuit model of the inductive strip by means of finite Q inductances that replace the ideal inductors of the lossless model. The accuracy of the model was justified by comparing the experimental and the predicted response of a X-band finline filter, that is simulated using the lossy circuit model of the inductive strip. The responses had the same shape with the

maximum discrepancy in the vicinity of 1 db. As a result, the accuracy of the inductive strip circuit model has been improved by incorporating the effect of the associated ohmic losses.

B. RECOMMENDATIONS

The model accounts for the loss associated with a thin centered inductive strip placed in homogeneous finline. It would be interesting to incorporate the effect of the dielectric losses in the circuit model of the inductive strip positioned in inhomogeneous finline, when such a model is developed.

APPENDIX A

The circuit file of X-band finline filter.

```
Touchstone (TM) - Configuration: 100 1700 101 16413 23ST 1000 ) '9582 '
                  LOSFF.CKT    Tue Aug 21 08:32:05 1990


! USER:       LEVENT KURTOGLU
! DATE:       30.5.90
! CIRCUIT:    FINLINE FILTER

! COMMENT:    THIS CIRCUIT MODELLES 3 RESONATOR 4 STRIP FILTER WITH ALL THE
!             LOSSES ARE INCLUDED.


DIM
  FREQ GHZ
  RES OH
  IND NH
  CAP PF
  LNG MIL
  TIME PS
  COND /OH
  ANG DEG

VAR
   A = 900
   B = 400
   Wovb = 1.00
   T1 = 90
   T2 = 253
   T3 = 240
   T4 = 90
   R1 = 553
   R2 = 540
   R3 = 540
   C = 0.0070

   pi = 3.1415?

   A1 = 13.25
   B1 = 10.01
   C1 = 1.621

   Q1=45    ! QUALITY FACTOR OF STRIP LEADING EDGE
   Q=5000   ! QUALITY FACTOR OF BEAM-CUTOFF SECTIONS
   F=10     ! THE FREQUENCY AT WHICH Q FACTORS ARE CALCULATED.

EQN

!  MODELLING STRIP LEADING EDGE

   w=2*pi*FREQ
   M = 2*B/A
   N = 1 - Wo.b
   Aov2 = A/2
   Aeq1 = 2 +    + Meo2 ** + Neo2 **2 E
   Aeq2 = 2.221 +  1 Meo2 E  + Neo2
   Aeq =  Aeq1 + Aeq2 **

   Aeq1 = 0.6 +  2 1E - 2 1247 + Meo1 25 + Meo2 **0 5
```

```
Touchstone (TM) - Configuration' 100 1700 101 16413 2357 1000 ' 15532 )
            LOSFF.CKT    Tue Aug 21 08:32:05 1990

   Beo2 = -0.17 + (1/M)**1.15 + N**10
   Beo = (Beo1 + Beo2)*8

   Lamda = (30000/2.54)/FREQ
   LpovL1 = 1/(1 - (Lamda/(2*Aeo))**2)**0.5
   LpovL2 = 1/(1 - (Lamda/(2*A))**2)**0.5
   Z1 = 120*pi*(2*Beo/Aeo)*LpovL1
   Z2 = 120*pi*(2*B/A)*LpovL2
   X1 = (Z1/Z2)**0.5

!  EQUATIONS FOR STRIP LEADING EDGE INDUCTANCES

   Ld1 = A1 + ((B1 - C1*ln(T1))/(1 + exp((T1 - 500)/10)))
   Ld2 = A1 + ((B1 - C1*ln(T2))/(1 + exp((T2 - 500)/10)))
   Ld3 = A1 + ((B1 - C1*ln(T3))/(1 + exp((T3 - 500)/10)))
   Ld4 = A1 + ((B1 - C1*ln(T4))/(1 + exp((T4 - 500)/10)))

!  MODELLING BELOW-CUTOF WAVEGUIDE SECTIONS

   Alfa=(2*pi/LAMDA)*(((LAMDA/(2*Aov2))**2-1)**0.5)
   Xo=(2*B/Aov2)*120*pi/(((LAMDA/(2*Aov2))**2-1)**0.5)

   Snh1=.5*(Exp(Alfa*T1)-(1/Exp(Alfa*T1)))
   Csh1=.5*(Exp(Alfa*T1/2)+(1/Exp(Alfa*T1/2)))
   Sinh1=.5*(Exp(Alfa*T1/2)-(1/Exp(Alfa*T1/2)))

   Snh2=.5*(Exp(Alfa*T2)-(1/Exp(Alfa*T2)))
   Csh2= 5*(Exp(Alfa*T2/2)+(1/Exp(Alfa*T2/2)))
   Sinh2= 5*(Exp(Alfa*T2/2)-(1/Exp(Alfa*T2/2)))

   Snh3= 5*(Exp(Alfa*T3)-(1/Exp(Alfa*T3)))
   Csh3= 5*(Exp(Alfa*T3/2)+(1/E p(Alfa*T3/2)))
   Sinh3= 5*(Exp(Alfa*T3/2)-(1/E p(Alfa*T3/2)))

   Snh4=.5*(Exp(Alfa*T4)-(1/E p(Alfa*T4)))
   Csh4=.5*(Exp(Alfa*T4/2)+(1/Exp(Alfa*T4/2)))
   Sinh4= 5*(Exp(Alfa*T4/2)-(1/Exp(Alfa*T4/2)))

!  EQUATIONS FOR BELOW-CUTOFF INDUCTANCES

   1L1=xo*Snh1/(Csh1*w)
   1L2=xo*Snh1/w
   1L12=2*1L2

   2L1=xo*Sinh2/(Csh2*w)
   2L2=xo/(Snh2*w)
   2L12=2*2L2

   3L1=xo*Sinh3/(Csh3*w)
   3L2=xo/(Snh3*w)
   3L12=2*3L2

   4L1=xo*Sinh4/(Csh4*w)
   4L2=xo/(Snh4*w)
   4L12=2*4L2
```

```
Touchstone (TM) - Configuration: 100 1700 101 16413 2357 1000 ( 15582 )
                LOSFF.CKT     Tue Aug 21 08:32:05 1990


CKT
!  LOSSLESS MODEL OF EACH STRIP

   IND    1   0   L^Ld1
   CAP    1   0   C^C
   IND    1   2   L^1L1
   IND    2   0   L^1L22
   DEF2P  1   2   A

   XFER   1   2    0    0    N^X1
   A      2   3
   A      2   3
   A      4   3
   A      4   3
   XFER   5   4    0    0    N^X1
   DEF2P  1   5   STRIP1

   IND    1   0   L^Ld2
   CAP    1   0   C^C
   IND    1   2   L^2L1
   IND    2   0   L^2L22
   DEF2P  1   2   B

   XFER   1   2    0    0    N^X1
   B      2   3
   B      2   3
   B      4   3
   B      4   3
   XFER   5   4    0    0    N^X1
   DEF2P  1   5   STRIP2

   IND    1   0   L^Ld3
   CAP    1   0   C^C
   IND    1   2   L^3L1
   IND    2   0   L^3L22
   DEF2P  1   2   C

   XFER   1   2    0    0    N^X1
   C      2   3
   C      2   3
   C      4   3
   C      4   3
   XFER   5   4    0    0    N^X1
   DEF2P  1   5   STRIP3

   IND    1   0   L^Ld4
   CAP    1   0   C^C
   IND    1   2   L^4L1
   IND    2   0   L^4L22
   DEF2P  1   2   D

   XFER   1   2    0    0    N^X1
   D      2   3
   D      2   3
```

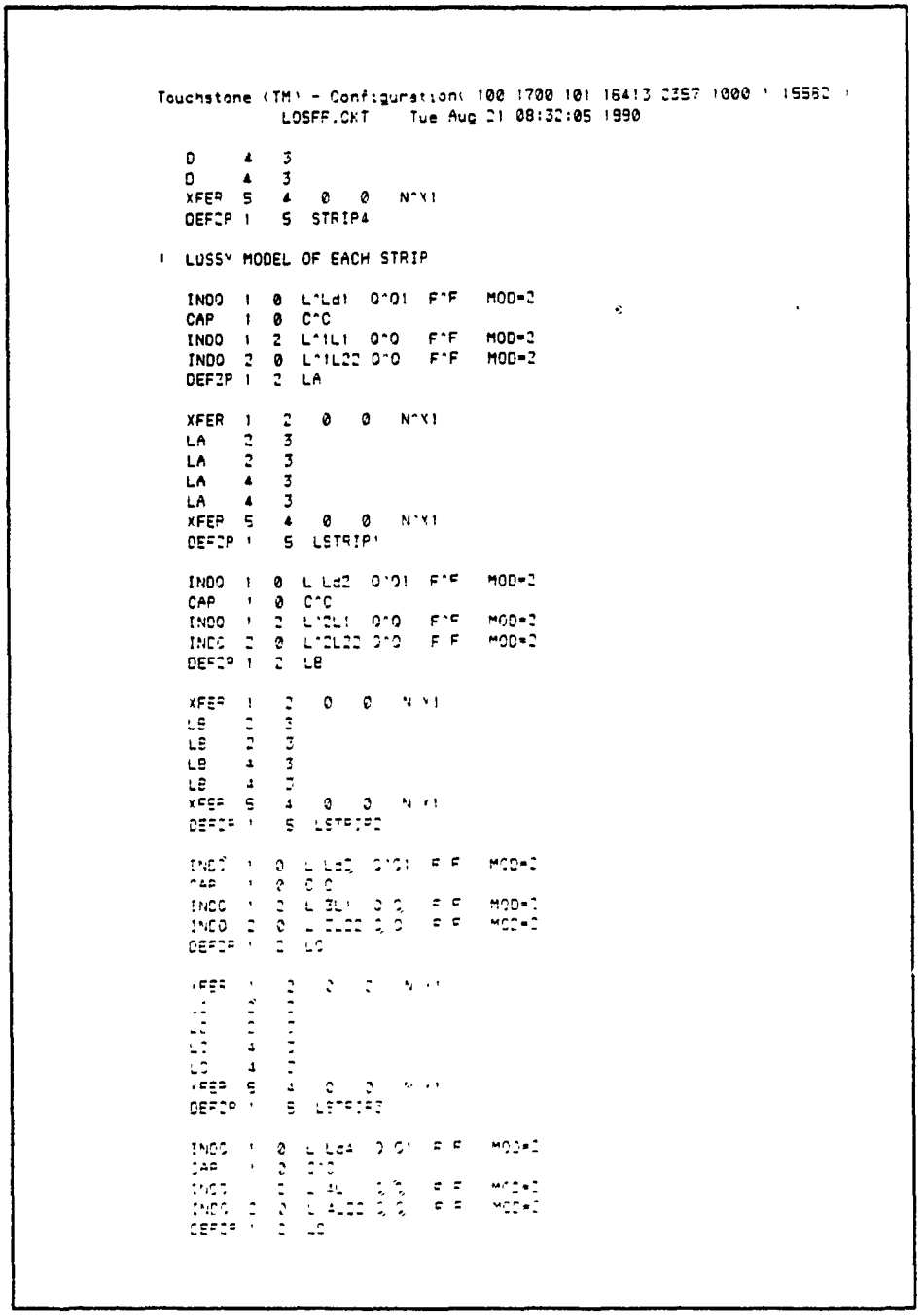

```
Touchstone (TM) - Configuration( 100 1700 101 16413 3357 1000 ' 15582 )
                LOSFF.CKT    Tue Aug 21 08:32:05 1990

   D     4   3
   D     4   3
   XFER  5   4   0   0   N^X1
   DEF2P 1   5  STRIP4

!  LOSSY MODEL OF EACH STRIP

   IND0  1   0  L^Ld1  0^01  F^F   MOD=2
   CAP   1   0  C^C
   IND0  1   2  L^1L1  0^0   F^F   MOD=2
   IND0  2   0  L^1L22 0^0   F^F   MOD=2
   DEF2P 1   2  LA

   XFER  1   2   0   0   N^X1
   LA    2   3
   LA    2   3
   LA    4   3
   LA    4   3
   XFER  5   4   0   0   N^X1
   DEF2P 1   5  LSTRIP1

   IND0  1   0  L Ld2  0^01  F^F   MOD=2
   CAP   1   0  C^C
   IND0  1   2  L^2L1  0^0   F^F   MOD=2
   IND0  2   0  L^2L22 0^0   F F   MOD=2
   DEF2P 1   2  LB

   XFER  1   2   0   0   N X1
   LB    2   3
   LB    2   3
   LB    4   3
   LB    4   3
   XFER  5   4   0   0   N X1
   DEF2P 1   5  LSTRIP2

   IND0  1   0  L Ld3  0^01  F F   MOD=2
   CAP   1   0  C^C
   IND0  1   2  L 3L1  0 0   F F   MOD=2
   IND0  2   0  L 3L22 0 0   F F   MOD=2
   DEF2P 1   2  LC

   XFER  1   2   0   0   N X1
   LC    2   3
   LC    2   3
   LC    4   3
   LC    4   3
   XFER  5   4   0   0   N X1
   DEF2P 1   5  LSTRIP3

   IND0  1   0  L Ld4  0 01  F F   MOD=2
   CAP   1   0  C^C
   IND0  1   2  L 4L   0 0   F F   MOD=2
   IND0  2   0  L 4L22 0 0   F F   MOD=2
   DEF2P 1   2  LD
```

```
Touchstone (TM) - Configuration '00 1700 101 16413 2357 1000 1 15582 %
            LOSFF.CKT    Tue Aug 21 08:32:05 1990

   XFER  1   2   0   0   N=X1
   LD    2   3
   LD    2   3
   LD    4   3
   LD    4   3
   XFER  5   4   0   0   N=X1
   DEFCP 1   5  LSTRIP4

!  DEFINING THE RESONATOR GAPS AND THE TEST CASE

   RWG   1  2  A=Aeq  B=Beq  L=R1  ER=1  RHO=1.64
   DEFCP 1  2  RES1

   RWG   1  2  A=Aeq  B=Beq  L=R2  ER=1  RHO=1.64
   DEFCP 1  2  RES2

   RWG   1  2  A=Aeq  B=Beq  L=R3  ER=1  RHO=1.64
   DEFCP 1  2  RES3

   RWG   1  2  A=Aeq  B=Beq  L=3846  ER=1  RHO=1.64
   DEFCP 1  2  FL

   RWGT  1  A=Aeq  B=Beq  ER=1  RHO=1.64
   DEFTP 1 WEDGE

!  LOSSLESS MODEL OF THE FINLINE FILTER

   FL      1  2
   STRIP1  2  3
   RES1    3  4
   STRIP2  4  5
   RES2    5  6
   STRIP3  6  7
   RES3    7  8
   STRIP4  8  9
   FL      9  10
   DEFCP   1  10 LOSSLESS

!  LOSSY MODEL OF THE FINLINE FILTER

   FL      1  2
   LSTRIP1 2  3
   RES1    3  4
   LSTRIP2 4  5
   RES2    5  6
   LSTRIP3 6  7
   RES3    7  8
   LSTRIP4 8  9
   FL      9  10
   DEFCP   1  10 LOSSY


TERM
   LOSSLESS WEDGE  WEDGE
   LOSSY    WEDGE  WEDGE
```

```
Touchstone (TM) - Configuration( 100 1700 101 16413 2357 1000 1 15582
              LOSFF.CFT    Tue Aug 21 08:32:05 1990


PROC

OUT
   LOSSLESS DB[S21] GR1
   LOSSY    DB[S21] GR1
   LOSSLESS DB[S11] GR1
   LOSSY    DB[S11] GR1

FREQ
   SWEEP  8  12  .1
   SWEEP  9.5  10.5  .01
GRID
   RANGE  8  12  0.4
   GR1   -60  20  10

OPT

TOL
```

The data file of X-band finline filter.

```
Touchstone (TM) - Configuration( 100 1700 101 16413 2357 1000 1 15592 )
                LOSFF.OUT     Tue Aug 21 08:20:07 1990

FREQ-GHZ  DB[S21]    DB[S21]    DB[S11]    DB[S11]
          LOSSLESS     LOSSY    LOSSLESS     LOSSY

 8.00000  -64.058   -64.137     -0.037     -0.120
 8.10000  -61.928   -62.013     -0.036     -0.135
 8.20000  -59.729   -59.821     -0.035     -0.141
 8.30000  -57.450   -57.550     -0.035     -0.149
 8.40000  -55.078   -55.186     -0.036     -0.158
 8.50000  -52.597   -52.714     -0.036     -0.169
 8.60000  -49.989   -50.118     -0.036     -0.180
 8.70000  -47.232   -47.375     -0.035     -0.194
 8.80000  -44.300   -44.458     -0.034     -0.210
 8.90000  -41.155   -41.334     -0.033     -0.231
 9.00000  -37.751   -37.956     -0.033     -0.259
 9.10000  -34.023   -34.264     -0.034     -0.300
 9.20000  -29.875   -30.170     -0.038     -0.363
 9.30000  -25.164   -25.543     -0.049     -0.469
 9.40000  -19.657   -20.190     -0.089     -0.694
 9.50000  -12.977   -13.852     -0.277     -1.279
 9.51000  -12.229   -13.159     -0.333     -1.391
 9.52000  -11.465   -12.456     -0.379     -1.522
 9.53000  -10.686   -11.744     -0.448     -1.674
 9.54000   -9.894   -11.026     -0.533     -1.853
 9.55000   -9.090   -10.303     -0.640     -2.062
 9.56000   -8.277    -9.579     -0.773     -2.310
 9.57000   -7.459    -8.855     -0.939     -2.604
 9.58000   -6.641    -8.139     -1.149     -2.954
 9.59000   -5.830    -7.434     -1.414     -3.373
 9.60000   -5.036    -6.748     -1.746     -3.875
 9.61000   -4.269    -6.087     -2.155     -4.477
 9.62000   -3.544    -5.461     -2.657     -5.199
 9.63000   -2.873    -4.878     -3.274     -6.065
 9.64000   -2.272    -4.341     -4.025     -7.102
 9.65000   -1.752    -3.860     -4.931     -8.338
 9.66000   -1.321    -3.444     -5.978     -9.806
 9.67000   -0.990    -3.095     -7.420     -11.533
 9.68000   -0.725    -2.799     -8.747     -13.553
 9.69000   -0.549    -2.548     -10.349    -15.895
 9.70000   -0.428    -2.352     -11.158    -17.593
 9.71000   -0.376    -2.210     -11.599    -18.430
 9.72000   -0.352    -2.097     -12.221    -17.946
 9.73000   -0.353    -2.012     -12.141    -16.782
 9.74000   -0.367    -1.946     -11.879    -15.841
 9.75000   -0.395    -1.895     -11.552    -14.902
 9.76000   -0.410    -1.853     -11.252    -13.992
 9.77000   -0.407    -1.816     -11.020    -13.090
 9.78000   -0.428    -1.781     -10.875    -12.871
 9.79000   -0.441    -1.745     -10.932    -12.409
 9.80000   -0.435    -1.708     -10.997    -12.288
 9.81000   -0.420    -1.668     -11.046    -12.295
 9.82000   -0.397    -1.625     -11.210    -12.402
 9.83000   -0.367    -1.581     -11.592    -12.585
 9.84000   -0.331    -1.535     -12.201    -12.804
 9.85000   -0.292    -1.487     -12.35     -13.001
 9.86000   -0.251    -1.440     -12.559    -14.100
```

```
Touchstone (TM) - Configuration 100 1700 101 16413 2357 1000 1 15582 1
                LOSFF.OUT    Tue Aug 21 08:30:07 1990

 9.87000   -0.209   -1.394  -14.686  -14.923
 9.88000   -0.170   -1.350  -15.955  -15.666
 9.89000   -0.135   -1.311  -17.542  -16.609
 9.90000   -0.107   -1.276  -19.532  -17.591
 9.91000   -0.086   -1.248  -21.947  -18.474
 9.92000   -0.074   -1.227  -24.277  -19.025
 9.93000   -0.073   -1.214  -24.582  -19.005
 9.94000   -0.083   -1.211  -22.341  -18.366
 9.95000   -0.105   -1.216  -19.630  -17.303
 9.96000   -0.139   -1.231  -17.295  -16.069
 9.97000   -0.186   -1.256  -15.382  -14.833
 9.98000   -0.243   -1.290  -13.804  -13.673
 9.99000   -0.311   -1.332  -12.498  -12.619
10.0000   -0.388   -1.382  -11.375  -11.674
10.0100   -0.472   -1.438  -10.427  -10.834
10.0200   -0.563   -1.501   -9.611  -10.087
10.0300   -0.658   -1.568   -8.907   -9.426
10.0400   -0.757   -1.638   -8.297   -8.841
10.0500   -0.857   -1.710   -7.766   -8.323
10.0600   -0.956   -1.783   -7.305   -7.866
10.0700   -1.054   -1.856   -6.904   -7.462
10.0800   -1.148   -1.927   -6.555   -7.108
10.0900   -1.238   -1.995   -6.253   -6.799
10.1000   -1.322   -2.059   -5.994   -6.527
10.1100   -1.400   -2.119   -5.772   -6.294
10.1200   -1.470   -2.173   -5.584   -6.094
10.1300   -1.531   -2.220   -5.428   -5.925
10.1400   -1.584   -2.261   -5.301   -5.785
10.1500   -1.626   -2.294   -5.202   -5.674
10.1600   -1.659   -2.319   -5.130   -5.589
10.1700   -1.679   -2.334   -5.083   -5.529
10.1800   -1.689   -2.342   -5.062   -5.496
10.1900   -1.686   -2.339   -5.066   -5.486
10.2000   -1.672   -2.329   -5.097   -5.502
10.2100   -1.646   -2.307   -5.154   -5.545
10.2200   -1.608   -2.277   -5.240   -5.614
10.2300   -1.559   -2.239   -5.357   -5.711
10.2400   -1.498   -2.190   -5.507   -5.838
10.2500   -1.427   -2.134   -5.694   -5.996
10.2600   -1.345   -2.071   -5.922   -6.188
10.2700   -1.254   -2.001   -6.195   -6.418
10.2800   -1.155   -1.927   -6.520   -6.691
10.2900   -1.051   -1.849   -6.902   -6.995
10.3000   -0.944   -1.771   -7.349   -7.327
10.3100   -0.835   -1.693   -7.862   -7.705
10.3200   -0.727   -1.619   -8.445   -8.109
10.3300   -0.621   -1.552   -9.095   -8.522
10.3400   -0.544   -1.499   -9.794   -8.919
10.3500   -0.475   -1.460  -10.407   -9.249
10.3600   -0.429   -1.441  -10.907   -9.461
10.3700   -0.411   -1.447  -11.114   -9.494
10.3800   -0.420   -1.480  -10.909   -9.310
10.3900   -0.453   -1.550  -10.295   -8.911
10.4000   -0.508   -1.655   -9.299   -8.329
10.4100   -0.575   -1.788   -8.074   -7.667
```

Touchstone (TM) - Configuration: 100 1700 101 16413 2357 1000 * 15582
LOSFF.OUT Tue Aug 21 09:30:07 1990

10.4200	-0.956	-1.982	-7.346	-6.928
10.4300	-1.210	-2.206	-5.383	-6.202
10.4400	-1.510	-2.468	-5.516	-5.511
10.4500	-1.853	-2.767	-4.753	-4.874
10.4600	-2.233	-3.097	-4.093	-4.299
10.4700	-2.644	-3.456	-3.527	-3.785
10.4800	-3.079	-3.839	-3.043	-3.333
10.4900	-3.533	-4.241	-2.633	-2.938
10.5000	-4.001	-4.659	-2.284	-2.594
10.6000	-8.690	-9.002	-0.674	-0.874
10.7000	-12.603	-12.780	-0.281	-0.406
10.8000	-15.714	-15.835	-0.150	-0.245
10.9000	-18.217	-18.313	-0.097	-0.178
11.0000	-20.264	-20.348	-0.071	-0.146
11.1000	-21.956	-22.034	-0.056	-0.131
11.2000	-23.361	-23.437	-0.048	-0.123
11.3000	-24.531	-24.606	-0.042	-0.119
11.4000	-25.500	-25.577	-0.039	-0.118
11.5000	-26.297	-26.376	-0.036	-0.119
11.6000	-26.942	-27.024	-0.035	-0.122
11.7000	-27.452	-27.536	-0.034	-0.125
11.8000	-27.839	-27.927	-0.034	-0.129
11.9000	-28.114	-28.206	-0.033	-0.133
12.0000	-28.286	-28.382	-0.033	-0.137

LIST OF REFERENCES

[1] P. J. Meier, "Integrated fin-line millimeter components, " IEEE Trans. Microwave Theory and Tech., vol. MTT-22, pp. 1209-1216, Dec. 1974.

[2] J. B. Knorr, "CAD models for inductive strips in homogeneous finline," technical report NPS62-90-007, Naval Postgraduate School, Monterey, CA, March 1990.

[3] J. B. Knorr and P. M. Shayda, " Millimeter-wave fin-line characteristics," IEEE Trans. Microwave Theory and Tech., vol. MTT-28, pp.737-743, July 1980.

[4] B. Kim, " A computation of fin-line impedance," M. S. thesis, Naval Postgraduate School, Monterey, CA December 1984.

[5] J. B. Knorr and J. C. Deal, "Scattering coefficients of an inductive strip in a finline: theory and experiment," IEEE Trans. Microwave Theory and Tech., vol. MTT-33, pp. !011-1017, Oct. 1985.

[6] J. C. Deal, "Numerical computation of the scattering coefficients of an inductive strip in a fin-line," M. S. thesis, Naval Postgraduate School, Monterey, CA August 1988.

[7] J. B. Knorr, "A CAD model for the inductive strip in finline," technical report NPS 62-88-013, Naval Postgraduate school, Monterey, CA, August 1988.

[8] G. F. Craven and C. K. Mok, "The design of evanescent mode waveguide bandpass filters for a prescribed insertion loss characteristic," IEEE Trans. Microwave Theory and Tech., vol. MTT-19, pp. 295-306, Mar. 1971.

[9] P. A. Rizzi, " Microwave Engineering Passive Circuits," pg. 202. Prentice-Hall, Inc., Englewood Cliffs, NJ, 1988.

[10] M. Morua, "A circuit model for an inductive strip in homogeneous finline," M. S. thesis, Naval Postgraduate School, Monterey, CA, June 1990.

INITIAL DISTRIBUTION LIST

		No. Copies
1.	Defense Technical Information Center Cameron Station Alexandria, Virginia 22304-6145	2
2.	Library, Code 52 Naval Postgraduate School Monterey, California 93943-5002	2
3.	Professor J. Knorr, Code EC/Ko Naval Postgraduate School Monterey, California 93943-5000	2
4.	Professor R. Janaswamy, Code EC/Js Naval Postgraduate School Monterey, California 93943-5000	2
5.	Deniz Kuvvetleri K.ligi Personel Sube Bsk.ligi Bakanliklar, Ankara/TURKEY	1
6.	Kara Harp Okulu K.ligi Kutuphanesi Bakanliklar, Ankara/TURKEY	1
7.	Deniz Harp Okulu K.ligi Kutuphanesi Tuzla, Istanbul/TURKEY	1
8.	Orta Dogu Teknik Universitesi Okul Kutuphanesi Bagdat, Ankara/TURKEY	1
9.	Bogazici Universitesi Okul Kutuphanesi Bebek, Istanbul/TURKEY	1
10.	Kamran Khan 1-C-4/11 Nazimabad, Karachi PAKISTAN	1
11.	Levent Kurtoglu Bulbulderesi Cad. 58/3 Kucukesat, Ankara/TURKEY	1